Tidally driven multiscale pore water flow in a creek-marsh system

Pei Xin,[1,2] Li-Rong Yuan,[3] Ling Li,[1,2] and D. A. Barry[4]

Received 10 October 2010; revised 10 May 2011; accepted 31 May 2011; published 20 July 2011.

[1] Intertidal wetlands are complex hydrological systems characterized by strong, dynamic interactions between coastal surface water and groundwater, driven particularly by tides. We simulated such interactions with a focus on three-dimensional, variably saturated pore water flow in a creek-marsh system that bordered a tidally dominated main channel. Simulated intratidal groundwater dynamics exhibited significant flow asymmetry with nonzero mean flow velocities over the tidal period. The tidally averaged flow led to pore water circulation with three dimensionality linked strongly to the marsh topography, over a range of spatial scales: near the creek bank, around the creek meander, and over long marsh sections inclined toward the main channel. Particle tracking revealed that time scales associated with these circulations differed by orders of magnitude. Under the simulated conditions, the creek served as the main outlet of the pore water circulation paths, especially those linked with infiltration into the upper marsh surface areas away from the main channel. Local net efflux, influenced by the creek channel curvature, varied along the creek but produced a total discharge largely proportional to the creek length. Water infiltrating the soil in the lower marsh surface areas away from the creek tended to discharge directly to the main channel. However, the total discharge to the main channel was much less than that into the creek. This study highlights the hydrological complexity of intertidal marshes and the need for further research on interactions among marsh morphology, hydrology, and ecology, which underpin the functionalities of these wetland systems.

Citation: Xin, P., L.-R. Yuan, L. Li, and D. A. Barry (2011), Tidally driven multiscale pore water flow in a creek-marsh system, *Water Resour. Res., 47*, W07534, doi:10.1029/2010WR010110.

1. Introduction

[2] Intertidal wetlands such as salt marshes are important ecological systems at the land-ocean interface [*Chapman*, 1960]. Highly productive with a range of plant species, salt marshes serve as essential habitats for many intertidal fauna and influence greatly the productivity of coastal waters through nutrient exchange [*Valiela and Teal*, 1979]. These wetlands play a critical role in maintaining coastal biodiversity. As an important part of the global biogeochemical cycle, salt marshes may act as carbon sinks, moderating greenhouse gas emissions and global warming [*Chmura et al.*, 2003]. Moreover, they function as filters of particles and contaminants in terrestrial water discharging to the sea, protecting coastal water quality [*Vernberg*, 1993]. Under the threat of sea level rise, the marshes provide protection for the coastal zone through adaptation [*D'Alpaos et al.*, 2007].

[3] Salt marshes are also complex hydrological systems characterized by strong, dynamic interactions between surface water and groundwater, which underpin wetland functionality. The linkage between the hydrological and ecological processes has been the center of numerous studies of salt marsh systems. The nutrient outwelling hypothesis, postulated in the early 1960s, suggested that a salt marsh typically exports nutrients to the coastal sea [*Teal*, 1962; *Valiela and Teal*, 1979]. With the marsh system (marsh soil and the embedded tidal creeks) treated as a "black box" [e.g., *Valiela and Teal*, 1979; *Valiela et al.*, 1980; *Harvey and Odum*, 1990], several studies have been carried out with measurements of nutrient fluxes at the inlet and outlet of the system to derive exchange rates. Tracer studies have also been carried out to examine the contribution of marshes to chemical enrichment in coastal waters [e.g., *Jordan and Correll*, 1985; *Tobias et al.*, 2001]. Although these studies provided useful large-scale information, the accuracy of the estimated exchange rates is affected by the dynamic and spatially variable flow in the marsh, which is not well understood.

[4] Among various other factors including evapotranspiration, precipitation, and inland flow, the tide provides the primary driving force on interacting surface water and groundwater flow and mass transport processes in a salt marsh (Figure 1). The marsh platform undergoes cycles of inundation and exposure driven by the tide, which leads to dynamic, complex pore water flow and solute transport in the marsh soil. Recent numerical studies based on

[1]National Centre for Groundwater Research and Training, School of Civil Engineering, University of Queensland, Queensland, Australia.
[2]Centre for Eco-Environment Modelling, State Key Laboratory of Hydrology-Water Resources and Hydraulic Engineering, Hohai University, Nanjing, China.
[3]School of Engineering, University of Sun Yat-Sen, GuangZhou, China.
[4]Laboratoire de technologie écologique, Institut d'ingénierie de l'environnement, Faculté de l'environnement naturel, architectural et construit, Ecole Polytechnique Fédérale de Lausanne, Lausanne, Switzerland.

0043-1397/11/2010WR010110

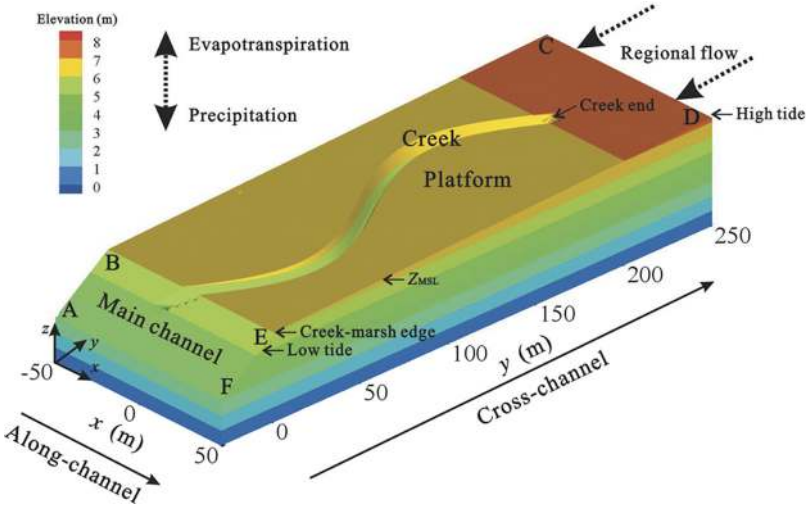

Figure 1. Diagram of the modeled creek-marsh system. ABCDEF represents the sediment surface where surface water and groundwater interacts. The contours show the marsh sediment elevation. The scale of the z axis is exaggerated by a factor of 8 relative to those of the x and y axes. Dashed arrows indicate forcing factors that were neglected in the present study.

two-dimensional (2-D) cross-creek section models showed that, during the early stage of inundation, surface water infiltrates the soil through the marsh platform. As the tide recedes, pore water seeps out of marsh sediments across the creek bank [*Ursino et al.*, 2004; *Gardner*, 2005; *Li et al.*, 2005; *Marani et al.*, 2006; *Wilson and Gardner*, 2006; *Xin et al.*, 2009]. Such intratidal flow dynamics generate net pore water flow in the form of circulation near the creek. This pore water circulation at the local scale provides a mechanism for more rapid solute exchange between the marsh soil and the tidal creek than that given by diffusive processes through the marsh surface. The circulation ultimately affects the overall nutrient exchange between the marsh and coastal water. These models also predicted improved soil aeration conditions in areas of rapid water circulation, as suggested by low phase-averaged (e.g., over a tidal period) soil water saturation [*Ursino et al.*, 2004; *Li et al.*, 2005; *Xin et al.*, 2009]. In other words, the optimal soil aeration condition tends to occur near the tidal creek. As the soil aeration condition affects plant root respiration and hence growth [*Mendelssohn et al.*, 1981; *Colmer and Flowers*, 2008], this result is consistent with previous observations that salt marsh plants such as *Spartina alterniflora* often grow better near tidal creeks than in the inner areas [*Mendelssohn et al.*, 1981; *Howes et al.*, 1981; *Howes and Goehringer*, 1994].

[5] Although the simulated pore water circulation was driven by the tidal forcing, the topographic change at the creek bank played a crucial role in generating the circulation. So far, modeling studies have been based on 2-D vertical marsh cross sections perpendicular to the creek [*Ursino et al.*, 2004; *Gardner*, 2005; *Li et al.*, 2005; *Marani et al.*, 2006; *Wilson and Gardner*, 2006; *Xin et al.*, 2010a], and have neglected the system's spatial variability and flow in the along-creek direction. In a real three-dimensional (3-D) salt marsh system, topographic variations would typically occur over a range of scales including, for example, significant slope changes at the creek (as represented in the 2-D model) and main channel, overall inclination of the marsh surface toward the main channel and shore, and creek meanders. Combined with tidal forcing, these topographic changes are also likely to generate pore water circulation over a range of scales. The multiscale pore water flow would influence significantly the marsh soil conditions (e.g., aeration and solute concentration) and the exchange between the marsh and coastal water. Therefore, a 3-D salt marsh model, including key topographic features at important scales, is needed for better characterization of the pore water flow in the marsh soil.

[6] The 3-D nature of the salt marsh system is inherent in the coupling of the surface water and groundwater flow and transport processes. Surface water and groundwater interactions have been examined in various environments (e.g., riparian and hyporheic zones, fluvial island, and estuary) at various scales (e.g., bed form, bar, bend, and basin) [*Smith and Turner*, 2001; *Cardenas*, 2008a, 2008b; *Cardenas*, 2009; *Francis et al.*, 2010]. Flow dynamics in these environments are affected mainly by adjacent rivers, whereas the flow and solute transport in a marsh are driven predominantly by and interact strongly with a tidally dynamic surface water flow system. A complex network of tidal creeks is embedded in marsh sediments, leading to interacting surface water and groundwater flow and solute transport that are 3-D in nature. The propagation of tides along these creeks creates spatially variable and temporally dynamic flow conditions in the creeks and over the marsh sediment surface (during overtopping). Such flow conditions not only provide the dominant forcing on subsurface flow and transport, but also induce complex surface transport pathways that control the net exchange between the marsh and coastal water.

[7] The aim of this study was to develop a 3-D model to investigate the interactions of surface water and groundwater in a creek-marsh system, with a particular focus on the tidally driven pore water flow in the marsh soil. A simplified 3-D marsh bordered with a main tidal channel was constructed with an embedded meandering creek. The marsh platform was inclined toward the main channel with a gentle slope (0.0048 for the base case). The creek-marsh system

was characterized by topographic (slope) changes over three different scales: (1) large slope changes at the creek and main channel banks, (2) marsh surface elevation changes associated with the creek meander, and (3) the small uniform inclination angle of the whole marsh platform. Numerical simulations of coupled surface water and groundwater flow were conducted using a recently developed modeling package [*Yuan et al.*, 2011] to examine the multiscale pore water flow in the modeled creek-marsh system. Particle tracking was used to elucidate the simulated flow characteristics, in particular, pore water circulation paths related to the tidally averaged flow and associated travel times.

2. Conceptual and Mathematical Models

2.1. Physical Conditions

[8] Accurate predictions of the hydrodynamics (surface and subsurface) in a real intertidal marsh system require detailed geomorphological and hydrogeological data, which are rarely available. With limited data, uncertainty in marsh topography and soil heterogeneity translates into uncertainties in direct comparisons between field data and model predictions. In this study a synthetic creek-marsh system (Figure 1) was constructed for simulations and characterization of tidally driven pore water flow in the marsh soil, with the aim to explore the role of the marsh topography in controlling the flow.

[9] The marsh was rectangular with a meandering creek and a main tidal channel included (Figure 1). For the base simulation (case 1), the marsh surface (BCDE; reference point coordinates are given in Table 1) had a plan dimension of 250 m (in the cross-channel direction y) $\times$ 100 m (in the along-channel direction x), and was inclined toward the main channel with a slope of 0.0048. The creek-marsh edge (BE) was connected to the main tidal channel with a surface section (ABEF) of 30 m $\times$ 100 m in plan dimensions and a slope of 0.1. The meandering creek was embedded in the marsh sediment, starting from $y = 0$ m (creek mouth) and extending to $y = 200$ m. The centerline of the creek followed a curve defined by $x = 20\sin(\pi y/100)$. The creek density given by the ratio of total channelized creek length (0.218 km) to marsh surface area (0.025 km^2) is 8.72 km km^{-2}. This creek density was set to be slightly smaller than those observed in the field [*Allen*, 2000; *Novakowski et al.*, 2004; *Torres and Styles*, 2007] as the modeled creek had a relatively high drainage capacity. Along the centerline, the creek bed elevation varied linearly from $z = 5$ m at the creek mouth to 5.96 m at the upper end, with the same slope (0.0048) as that of the marsh surface. In reality, the creek bed slope may be greater than the marsh surface slope, causing the creek depth to decrease with the distance from the main channel [*Torres and Styles*, 2007]. The creek's cross section was trapezoidal with a height of 1 m, and bottom and topside lengths equal to 2 and 12 m, respectively. At the upper end of the creek, a bevel side was set with the same slope as that of the local cross section. The modeled marsh topography including the surface elevation changes and creek configuration, although simplified, reflects geomorphologic characteristics of real salt marshes to some extent [*Rinaldo et al.*, 2004; *Torres and Styles*, 2007]. In particular, the 3-D topographic variations included in the model enables simulations of 3-D complex behaviors of pore water flow in response to tidal surface water oscillations, which have not been represented in previous numerical studies based on 2-D cross-creek sections [*Ursino et al.*, 2004; *Gardner*, 2005; *Li et al.*, 2005; *Wilson and Gardner*, 2006]. It should be noted that, despite the salt marsh background of the study, the synthetic model bears similarity to other intertidal systems, particularly upper sections of tidal flats.

[10] The marsh soil (sandy loam) was assumed to be hydraulically uniform and isotropic, with an impermeable horizontal base ($z = 0$). A single-constituent, sinusoidal tide was specified at the main channel boundary (AF in Figure 1) as the forcing condition in the model, i.e.,

$$h(t) = Z_{\mathrm{MSL}} + A\cos(\omega t), \tag{1}$$

where $h(t)$ is the specified water level [L] at the time t [T]; Z_{MSL} is the mean sea level [L]; and A and ω are the tidal amplitude [L] and angular frequency [T^{-1}], respectively. The tide propagated toward the marsh, causing submersion and emersion of the marsh platform during the rising and falling tidal phase, respectively. The creek acted as a subchannel of rapid transmission for the tidal signal, and thus played an important role in modulating the response of the marsh to the tide.

2.2. Coupled Surface Water and Groundwater Flow Model

[11] A coupled model based on ELCIRC for surface water flow and solute transport [*Zhang et al.*, 2004] and SUTRA for groundwater flow and solute transport [*Voss and Provost*, 2008] was employed to simulate the interactions between surface water and groundwater in the modeled salt marsh driven by the tide. The details of the coupling approach and model validation can be found in *Yuan et al.* [2011]. While the coupling of the surface water and groundwater is not particularly needed for the flow simulation, such coupling is essential for modeling chemical transport and reactions in the marsh system, especially for chemicals that are sourced from the marsh soil, which will be investigated in future studies. Here we recap briefly the processes simulated by the model and the approach used for surface water and groundwater coupling.

[12] Tidal propagation in the surface water of the modeled system behaved essentially like long waves; and thus the resulting flow and water level fluctuations were well described by the shallow-water equations used in the ELCIRC model (details in *Zhang et al.* [2004]). The variably saturated pore water flow in the marsh soil was governed by the Richards' equation as used in SUTRA [*Voss and Provost*, 2008].

Table 1. Coordinates of Reference Points (Shown in Figure 1) of the Model Domain (x, y, z)

A (m)	B (m)	C (m)	D (m)	E (m)	F (m)
(−50, −30, 3)	(−50, 0, 6)	(−50, 250, 7.2)	(50, 250, 7.2)	(50, 0, 6)	(50, −30, 3)

[13] For the sandy loam soil type (typical of some salt marshes [*Simonini and Cola*, 2002]) considered in this study, the compressibility of water and soil matrix played only a minor role in the pore water flow in the marsh soil [*Wilson and Gardner*, 2006; *Xin et al.*, 2009] and thus was neglected in the simulation. Then, the varying total stress on the marsh platform due to the water depth variations during the submergence requires no special treatment [*Yuan et al.*, 2011]; otherwise Richards' equation needs to be modified to include a tidal loading term [*Reeves et al.*, 2000]. Note that proper simulation of the unsaturated flow is essential because this flow is directly responsible for recharging the shallow groundwater system in the marsh soil and forms part of the intertidal pore water circulation as shown in section 3.

[14] The two submodels were coupled spatially at the common interface between the surface water and groundwater bodies (on marsh surface ABCDEF in Figure 1). Note that the intersections of the surface water level with the marsh surface varied temporally due to the tide, creating moving boundaries for the surface water model. In response, the boundary conditions of the groundwater model at the marsh surface also varied temporally. At the interface (submerged area), the specified water pressure on the boundary of the groundwater model fluctuated with the surface water level. Seepage faces formed and evolved dynamically above the surface water's moving boundaries. Beyond the seepage face was the unsaturated zone where no flux was permitted across the boundary. The surface water level computed by the ELCIRC model was used to determine the boundary condition at the interface of the groundwater model (SUTRA). In turn, the groundwater model provided water flux for the continuity equations of surface water flow to account for the mass exchange across the interface. Additionally, flux from the seepage face was routed instantaneously to the nearest surface water body according to the local marsh surface slope (i.e., the flux added directly to the nearest surface water cell, details in *Yuan et al.* [2011]). This simple routing method assumes that the seepage face is continuous and thus seepage water does not reinfiltrate the soil on the way to the surface water body. While the assumption is valid for the current modeled creek-marsh system, discontinuous seepage faces interspersed with unsaturated pockets may develop in marshes of more complex topographies and subjected to evaporation, in which case further development of the routing scheme is needed.

2.3. Initial and Boundary Conditions

[15] For the surface water modeling, initial flow velocities at all nodes were set to be zero and water levels at the maximum tidal height ($z = 7.3$ m). Correspondingly, the initial head condition for the groundwater model was set according to the hydrostatic pressure given by the surface water level at the high tide.

[16] For the surface water model, no-flow boundaries were used for sides ABC, CD, and DEF. While the no-flow condition might represent symmetry boundaries at sides ABC and DEF, side CD permitting no flow but with a water depth of 0.1 m at the high tide could be thought as being confined by a levee. At the main channel boundary (AF), the surface water level was specified according to the harmonic astronomical tide (equation (1)). As discussed earlier, the surface water level predicted by ELCIRC was used to drive pore water flow in the marsh soil. For each node at the interface (ABCDEF), (1) if the node was treated as being dry by ELCIRC (water depth less than a preset threshold value) and with a negative pore water pressure calculated from SUTRA at the previous time step, it was taken as a no flow boundary; (2) if the node was treated as being dry by ELCIRC and with a positive pore water pressure calculated from SUTRA at the previous time step, it was taken as part of a seepage face and specified with the atmospheric (zero) pressure [*Wilson and Gardner*, 2006]; and (3) if the node was treated as being wet (inundated) by ELCIRC, it was taken as a specified-head boundary subjected to hydrostatic pressure given by the local water depth (details in *Yuan et al.* [2011]). The side boundaries of the groundwater model along ABC and DEF were assumed to be hydraulic divides and thus set as no flow boundaries. With the regional groundwater flow neglected, side CD was also set as a no flow boundary.

2.4. Values of Key Physical Parameters and Discretization Used in the Simulation

[17] Sandy loam, a typical soil type encountered in salt marshes, was used as the simulated marsh soil [*Simonini and Cola*, 2002]. Following *Wang et al.* [1997], the porosity ϕ was set to 0.445. The values of the saturated hydraulic conductivity K_s (1.23×10^{-5} m s^{-1}), the residual water saturation $S_{W\mathrm{res}}$ (0.146) and the *van Genuchten* [1980] water retention parameters n (1.89) and α (7.5 m^{-1}) were from *Carsel and Parrish* [1988].

[18] For the surface water modeling, the Manning roughness coefficient, which affects the tidal signal propagation in the marsh system, was set to 0.015 uniformly for the creek (bank and bed), main channel (bank), and the marsh platform. In real salt marshes, plants distributed on the marsh surface provide nonuniform resistance to the flow and thus modify the values of local roughness coefficient. Moreover, plant zonation correlated with the marsh topography would lead to complex patterns of roughness variations, which may affect the local surface water depth, and hence surface water and groundwater flow interactions. However, as a first attempt to examine the 3-D characteristics of pore water flow in the marsh soil, this study neglected these effects.

[19] The tide was set with an amplitude of 1 m and period of 12 h (semidiurnal solar tide; $\omega = \pi/6$ rad h^{-1}). The mean sea level was set to be 6.3 m. Under such a tidal regime, the marsh platform was completely inundated at the high tide with a minimum water depth (at the marsh top) equal to 0.1 m. At the low tide, the whole marsh platform emerged; however, a small part of the creek near the main channel was still flooded with relatively shallow water depths (0 to 0.3 m).

[20] In the numerical simulation, the marsh surface together with the main channel (ABCDEF) was represented by 8736 elements (8927 nodes) horizontally. The 3-D mesh of the groundwater domain was constructed to reflect the marsh topography. In particular, the groundwater domain was vertically divided into 30 layers across the whole area. As indicated by previous numerical studies, pore water flow varies the most near the creek [*Li et al.*, 2005; *Wilson and Gardner*, 2006; *Xin et al.*, 2009]. Thus the mesh was refined in the near-creek area with smaller grid sizes, around 0.4 m (in the x direction) compared with 1 m for

grids in areas away from the creek. A time step of 10 s was used in the groundwater model and 1 s for the surface water model (different time steps were used in the two models for computational efficiency as discussed in *Yuan et al.* [2011]). Tests on the simulation's independence of time step and mesh size demonstrated the convergence of the numerical solutions. Furthermore, the simulation was run for a relatively long time period (4 tidal periods) to ensure that the numerical solutions reached a quasi-steady state (i.e., periodic solutions unaffected by the initial condition).

3. Results of the Base Simulation

3.1. Temporal Dynamics and Spatial Variations of Pore Water Flow

[21] We first examined the simulated pore water flow in the surface soil layer (around 0.1 m deep, top elements in the numerical model) at a rising and a falling tidal stage, respectively (Figure 2). The flow was generally 3-D and varied with the tide, particularly in the near-creek area. As the tide rose and inundated the marsh platform, significant infiltration across the marsh surface occurred near the surface wetting front (intersection of the surface water level with the sediment surface; Figure 2a). In lower areas from the wetting front to the main channel, the marsh soil became fully saturated after a period of inundation and experienced very weak flow. In contrast, the upper area landward of the wetting front was still draining to the creek (hereinafter "landward" refers to the direction toward the upper boundary of the model). Close to the wetting front, drainage across the marsh surface also occurred, forming a seepage face on the platform. As the tide propagated further inland in the creek, the rise of the creek water level led to infiltration (to the marsh soil) across the bank and

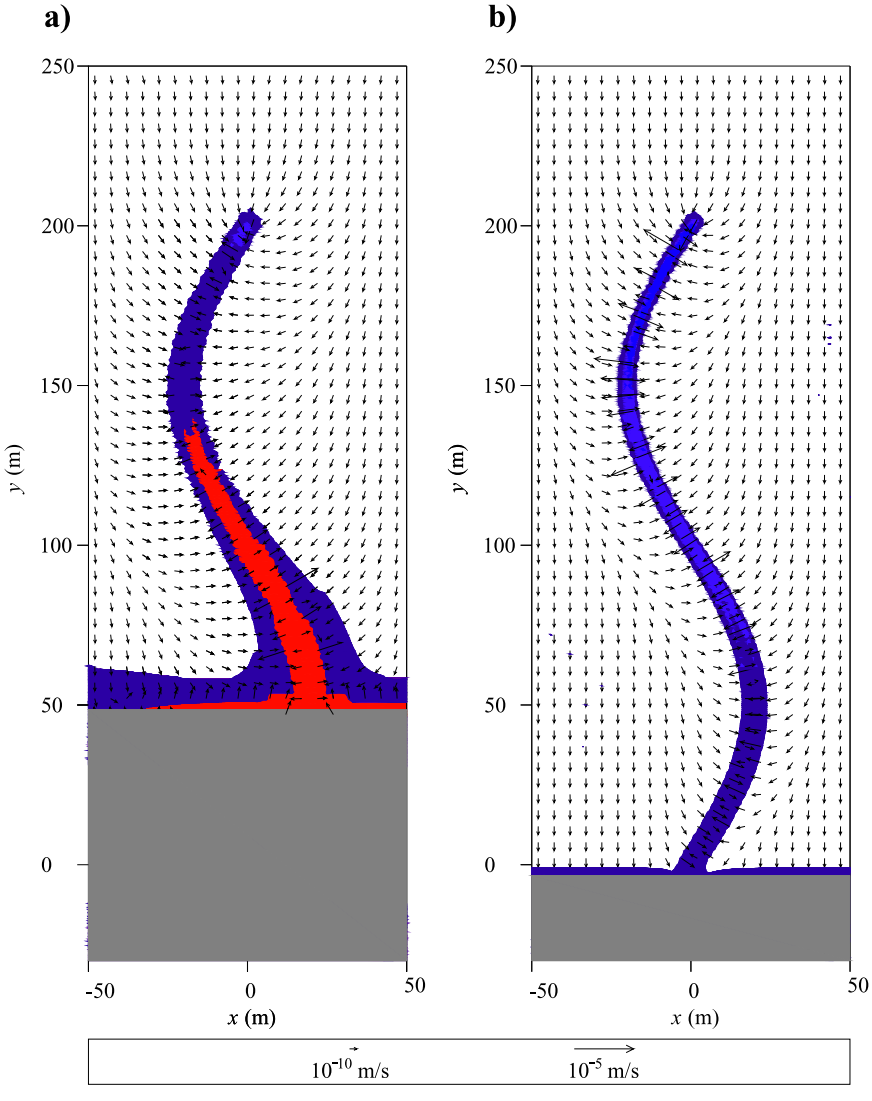

Figure 2. Horizontal (vector) and vertical flow during (a) the rising tide (elapsed time 9 h) and (b) the falling tide (elapsed time 4 h). Blue shows surface areas of upward flow; red indicates surface and creek bed areas of downward flow at the beginning of the submersion; and gray color represents weak flow areas under inundation. In both cases, the whole creek bed was inundated. Note that the size of arrow for velocity vector of a magnitude between the minimum and maximum values is scaled linearly between the two arrows shown in the box; and for Figure 2b, long arrows on one side of the creek extended to the other side.

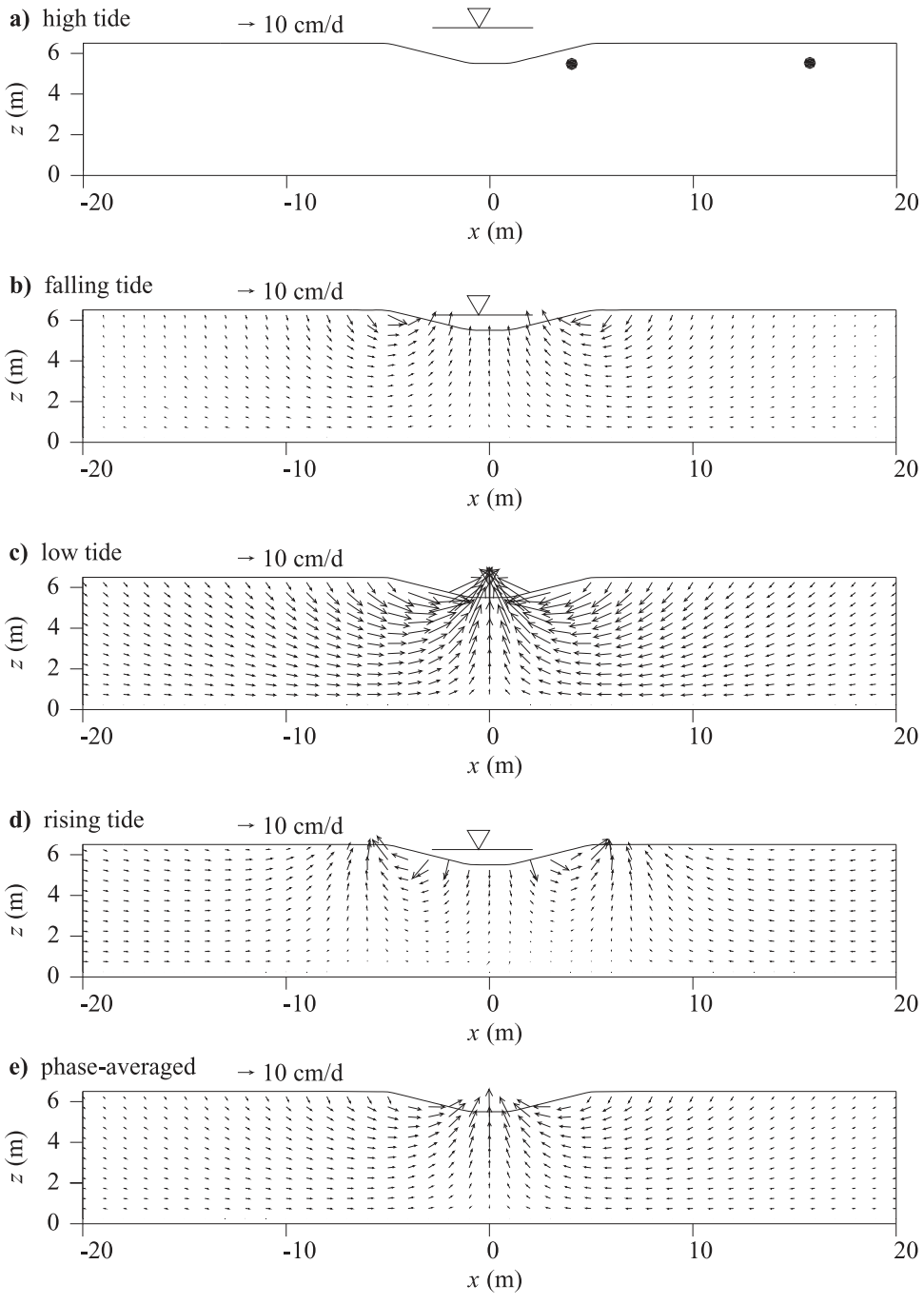

Figure 3. Vertical flow velocity field for (a) high tide (elapsed time 0 h), (b) falling tide (elapsed time 3 h), (c) low tide (elapsed time 6 h; note that the creek was dry at the time), (d) rising tide (elapsed time 9 h), and (e) phase-averaged result. All plots show 2-D flow in a cross-section parallel to the main channel ($y = 100$ m). The two solid circles in Figure 3a indicate the observation points for Figure 4. The surface water level (above the creek bed) is also indicated.

through the bed landward of the surface wetting front. During the falling tide the exposed marsh area drained mainly to the creek. Drainage also occurred through the seepage face on the marsh platform, which formed landward of the retreating surface wetting front. As the main channel emerged, a narrow seepage face formed on the relatively steep channel bank (Figure 2b). During both the rising and falling tides, the pore water flow was significantly affected by the creek meander.

[22] To examine the flow characteristics in detail, we selected two vertical sections: one across the creek and midway up from the main channel (at $y = 100$ m), and the other perpendicular to the main channel and 10 m from the side boundary ABC (at $x = -40$ m). Simulated flow in the cross-creek section at different tidal stages is shown in Figure 3. The pore water flow velocities at high tide were very low (Figure 3a), indicating that the pore water pressure in the saturated marsh soil was largely uniform and hydrostatic. As the tide receded, pore water flow developed toward the creek; and the flow activity was weakened with increasing distance from the creek (Figure 3b). The drainage to the creek intensified at the low tide (Figure 3c). At this stage, the local creek was without any surface water as the tidal water level had retreated almost to the main channel. However, ongoing exfiltration from the marsh soil maintained the wetness of the creek bed as part of the seepage face. A large part of the exposed creek bank and bed during the falling tide remained wet as it provided the drainage area for the pore water exiting the marsh soil. As the tide rose, infiltration (from the creek to the marsh soil) occurred below the intersection of the tidal water level with the creek bank (Figure 3d). This infiltration combined with the drainage process in the inner marsh area led to an upward flow near the creek bank (Figure 3d). These intratidal flow dynamics were characterized essentially by dominant infiltration through the marsh platform and drainage across the creek bank and bed. Note that while infiltration occurred across the creek bank during the rising tide (Figure 3d), the exfiltration dominated over the tidal period. This led to a tidally averaged flow in the form of circulation near the creek bank (Figure 3e), a phenomenon that has been shown by previous studies based on 2-D models [*Wilson and Gardner*, 2006; *Xin et al.*, 2009].

[23] Although only flow velocities in the x and z directions are shown in Figure 3, the flow along the selected cross-creek transect was clearly 3-D. To demonstrate this, local velocities in the x, y, and z directions were plotted for three observation points along the transect: first just under the creek bank (indicated in Figure 3a: $x = 4.02$ m, $y = 100$ m, $z = 5.48$ m), second near the creek bank (indicated in Figure 3a: $x = 15.74$ m, $y = 100$ m, $z = 5.53$ m) and third in the inner marsh area ($x = 48.61$ m, $y = 100$ m, $z = 5.53$ m; not in the range shown by Figure 3a). At the observation point under the creek bank (Figure 4b), the cross-creek flow velocity (v_x) had a larger magnitude than those of the cross-channel (v_y) and vertical flow velocities (v_z). As the distance from the creek increased, the magnitudes of all three velocity components decreased (Figures 4c and 4d), indicating weakening flow in the inner marsh area. The overall flow patterns at the first two locations (near the creek) were characterized by a prolonged drainage phase that started as the tidal water level fell below the local marsh platform elevation (around 2.6 h) and a rapid flow reversal phase as the rising tide approached (around 9.4 h). The flow reversal phase is apparent in the change of the vertical flow velocity. As the water level rose, infiltration across the creek bank occurred as shown in Figure 3d. This infiltration blocked the drainage of the inner area, forcing the pore water near the creek bank to flow upward (Figures 4b and 4c). As the water level overtopped the marsh platform, infiltration occurred with a rapid change of flow direction from upward to downward. Subsequently the flow ceased while the inundation continued. In the inner marsh area, downward flow persisted during the period of platform exposure with an increased flow rate associated with infiltration at the instant of overtopping (Figure 4d). It is interesting that the cross-channel flow (v_y) at this location, driven essentially by tide-induced cross-channel hydraulic gradients on the sloping channel bank, appeared to dominate over the cross-creek flow (v_x), in contrast to the trend shown in Figure 4b. This indicated relatively weak influence of the creek on the flow in the marsh interior.

[24] Focusing on the section perpendicular to the main channel at $x = -40$ m, we also examined flow on the y-z plane away from the creek. Intratidal flow around both rising and falling midtides differed from the flow on the cross section (Figures 5b and 5d). In particular, exfiltration occurred on the exposed sediment surface just above the tidal water level, which formed a seepage face. This exfiltration was due to the drainage of the marsh surface, which inclined toward the main channel (at a relatively small angle). At all tidal stages except the high tide, the flow activity concentrated near the instantaneous shoreline (intersection of the surface water level with the sediment surface). The intratidal flow dynamics also led to a phase-averaged, cross-channel circulation system (Figure 5e). These flow characteristics are similar to those of the beach groundwater system, where a near-shore area similar to the main channel bank exists [*Mao et al.*, 2006; *Robinson et al.*, 2007, *Robinson et al.*, 2009; *Xin et al.*, 2010b]. However, the cross-channel pore water circulation in the creek-marsh system was complicated by the influence of the creek, especially in the near-creek area as discussed further in section 3.2.

[25] To examine the overall hydraulic conditions in the marsh soil, we calculated the mean hydraulic head averaged over the sediment depth and tidal period, and the mean head gradient. The head variations were strongly linked to the marsh topography (Figure 6a). The mean head decreased toward the main channel, corresponding with the overall inclination of the marsh surface. Such a correspondence is commonly observed in shallow groundwater systems where the water table, receiving surface water recharge due to rainfall, typically varies with the topography of the land surface [*Alley et al.*, 2002; *Cardenas*, 2008a]. In the modeled creek-marsh system, the recharge occurred as a result of infiltration during the overtopping of the marsh platform, as evident in Figure 6b, which shows the difference between tidally averaged hydraulic heads at the sediment surface and base. The influence of the creek on the mean head was profound, leading to modifications of the head variations with decreasing trends toward the creek. This behavior is also a characteristic of shallow groundwater systems with "gaining" streams/rivers [*Alley et al.*, 2002; *Cardenas*, 2008a; *Cardenas*, 2009].

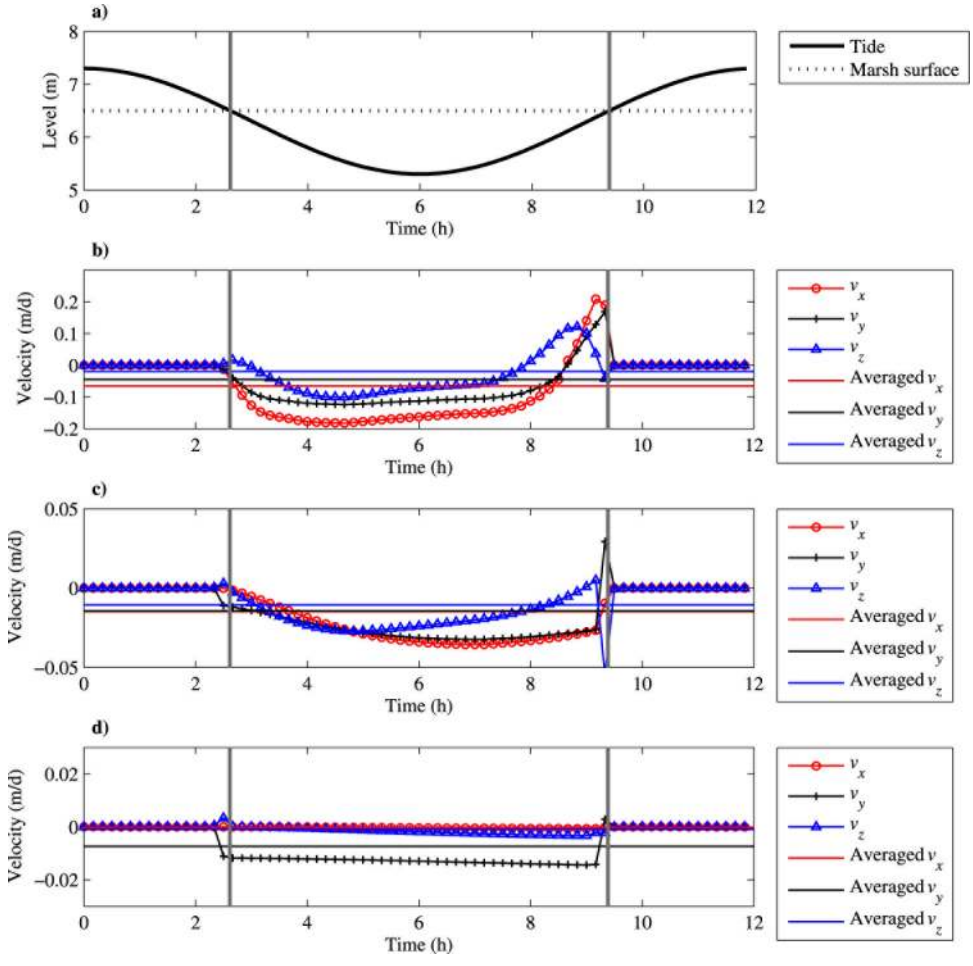

Figure 4. (a) Tidal water level fluctuation relative to the marsh surface elevation at the section of $y = 100$ m. Pore water flow velocity over a tidal period at (b) $x = 4.02$ m, $y = 100$ m, and $z = 5.48$ m; (c) $x = 15.74$ m, $y = 100$ m, and $z = 5.53$ m; and (d) $x = 48.61$ m, $y = 100$ m, and $z = 5.53$ m. The two vertical lines show the emersion period. Two observation points for Figures 4b and 4c are indicated in Figure 3a.

Although infiltration also occurred across the creek bank and bed on the rising tide, the creek served mainly as a key drainage outlet for pore water in the marsh soil over the tidal period. The overall mean flow pattern was characterized by infiltration (recharge) through the sediment surface, and exfiltration (drainage) across the creek bank and bed, and through the channel bank (Figure 6).

3.2. Particle Traces and Associated Travel Times

[26] To elucidate further the 3-D groundwater flow, the traces and travel times of passive particles moving through the marsh soil were calculated. The trace tracks the particle's movement driven by the flow in the marsh soil from the release point to the exit while the travel time measures the duration of the movement. Both quantities not only help to illustrate the pore water flow patterns but also provide information about the extent of contact between pore water/solute and soil grains, which would be useful for understanding the fate of chemicals transported through the marsh soil. As demonstrated by *Xin et al.* [2010b], particles in a groundwater system subjected to periodic forcing such as the tide move along oscillatory trajectories as given by the instantaneous flow field; however, the averaged flow controls the mean paths and associated travel times of the particles. Here we determined the traces and travel times of particles based on the tidally averaged pore water flow velocities. Particles were released to the surface soil layer at a depth of 0.5 m. Thus the results represent the behavior of "body circulation" that occurred underneath the surface layer as proposed by *Billerbeck et al.* [2006].

[27] First, we examined the behavior of particles released at various locations along a cross-creek transect at $y = 90$ m ($z = 5.93$ m). All the particles went through 3-D paths (Figures 7a and 7b), most of them moving downward initially and then upward to leave the sediment (Figure 7a). Near the creek, particles moved through a relatively shallow and short path, and exited the sediment to the creek within a short period. This path represents a pore water circulation system near the creek bank, similar to that found in previous studies based on 2-D cross-creek section models [*Wilson and Gardner*, 2006; *Xin et al.*, 2009]. As the distance from the creek increased, the particle on the right side took a diverted path to exit downstream (toward the main channel from the particle release location) to a

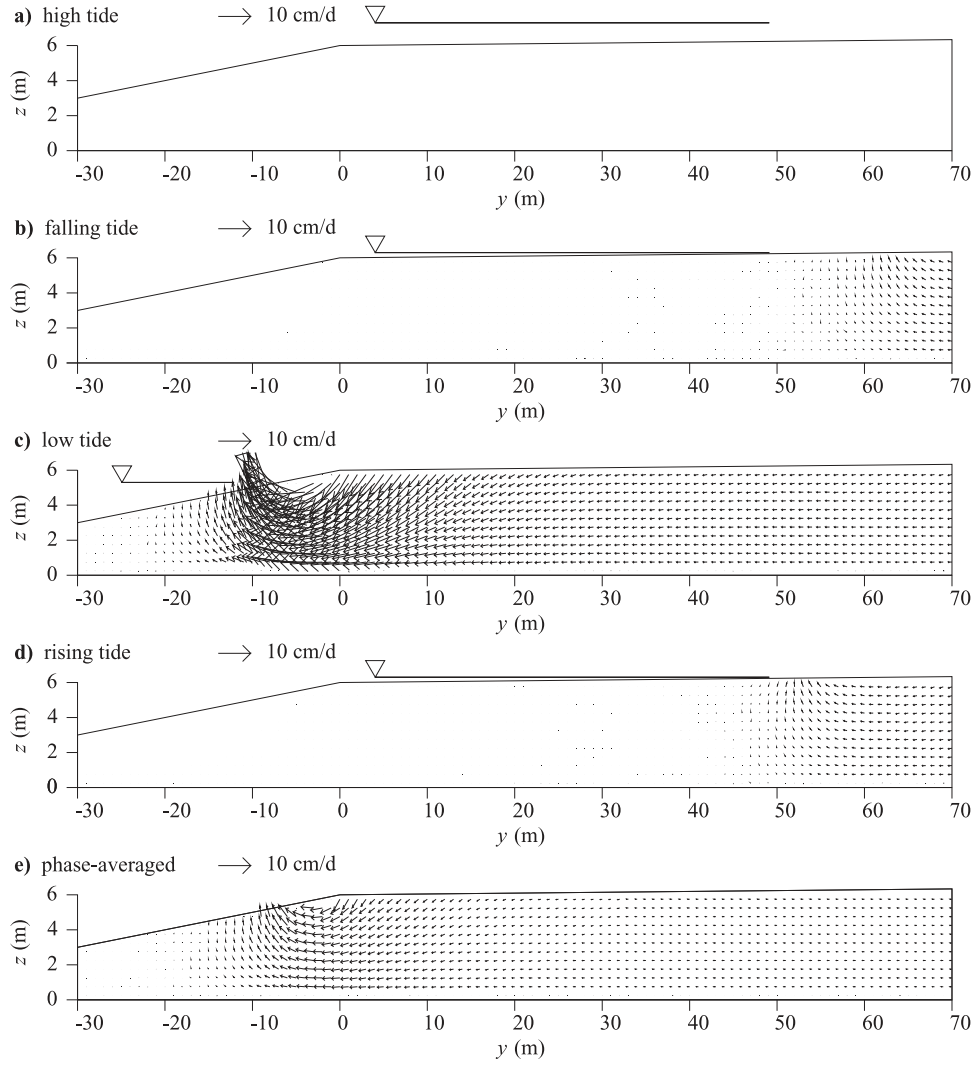

Figure 5. Flow velocity field for (a) high tide (elapsed time 0 h), (b) falling tide (elapsed time 3 h), (c) low tide (elapsed time 6 h), (d) rising tide (elapsed time 9 h), and (e) phase-averaged result. All plots show the 2-D flow at a cross section perpendicular to the main channel ($x = -40$ m). The surface water level is also indicated.

concave creek section. The associated pore water circulation was affected significantly by the creek meander. By comparison, the particles on the left side were less affected by the meander, which curved outward. Further away from the creek on the left side, the particle did not reach the creek but instead exited the marsh soil through the main channel bank (Figure 7b). This particle path demonstrated the three dimensionality of the cross-channel circulation shown in Figure 5a. While the circulation was predominantly driven by cross-channel hydraulic gradients due to the tidal water level oscillations on the inclining marsh surface, the influence of the creek was clearly visible.

[28] The travel times of these particles through the paths varied by three orders of magnitude (Figure 7c). While the particle initially placed at $x = 0$ m and $y = 90$ m traveled through a near-creek path to exit at the creek within 47 days, it took the particle released far away from the creek ($x = 40$ m and $y = 90$ m) 2185 days to travel to the creek downstream ($y = 68.5$ m). It took even longer (14590 days) for the particle initially placed at $x = -40$ m and $y = 90$ m to move through a cross-channel path and exit from the main channel bank.

[29] Further particle tracking was conducted with a large number (2397) of particles released uniformly to the surface soil layer. The results showed that most particles (2178 out of 2397) exited the soil at the creek (Figure 8a). Particles initially released close to the creek were drawn to nearby creek sections. Particles released away from the creek in the upper marsh surface areas were also drawn to the creek at sections downstream. Only a relatively small number of particles (219 out of 2397) initially released in the areas near the main channel and away from the creek exited the marsh soil through the channel bank (indicated by the white lines in Figure 8a). The creek appeared to have been responsible for draining ~91% (2178/2397) of the total marsh area. To explore further the link between particle tracking, pore water flow, and solute transport, we adjusted the number of released particles proportionally to

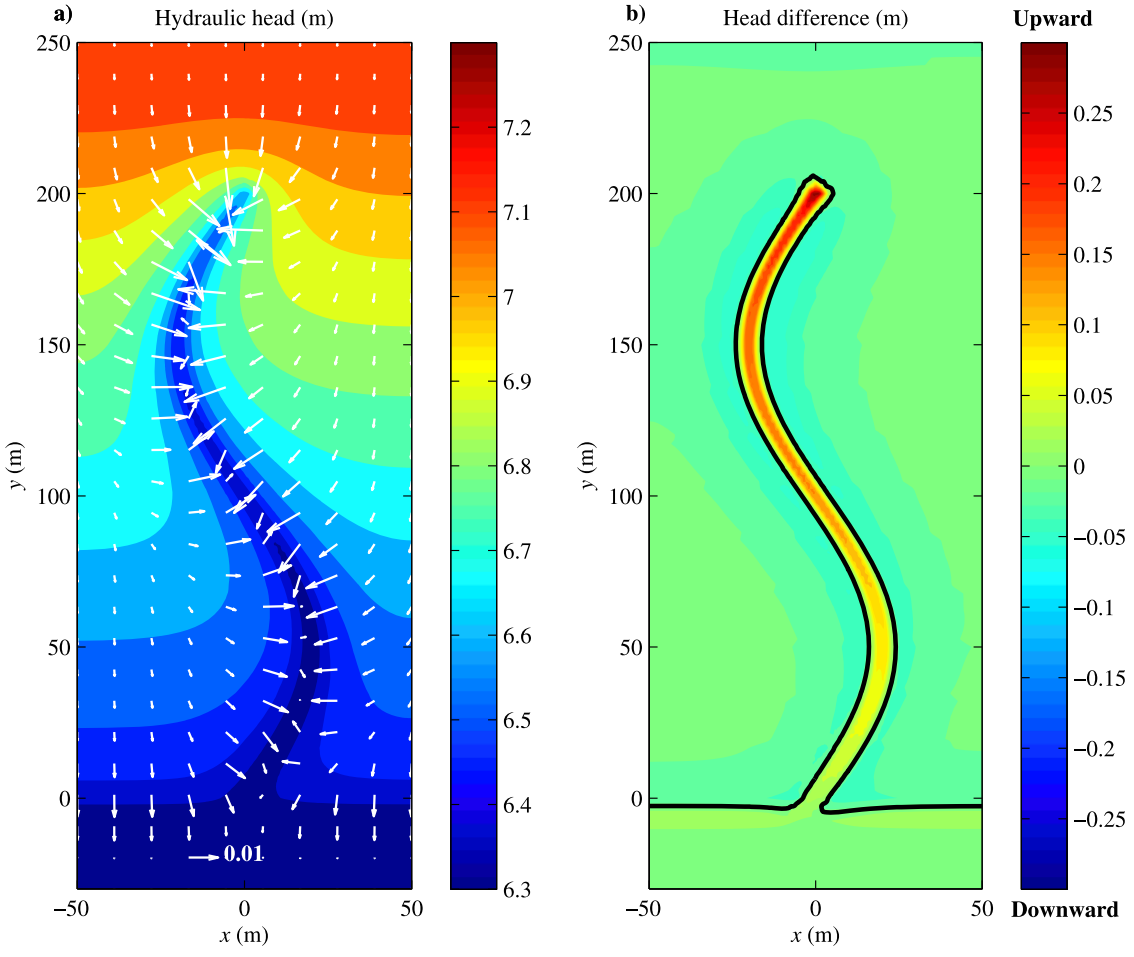

Figure 6. (a) Mean hydraulic head averaged over the sediment depth and tidal period. The vector field shows the horizontal hydraulic head gradient. (b) Difference between tidally averaged hydraulic heads at the sediment surface and base, indicative of the averaged vertical flow. The colored contours reflect the magnitude and direction of the flow: positive for upward flow and negative for downward flow. The black line in Figure 6b is the zero-value contour.

local tidally averaged infiltration rate. This flux-weighting adjustment reflects different mass fluxes represented by particles released at different places. The result showed that the creek provided the exit for 89% flux-weighted particles, implying that infiltrating water through the marsh surface was largely drained to the creek.

[30] The variations of the particle travel time exhibited an interesting spatial distribution that indicated marsh areas associated with rapid and slow pore water circulation (Figure 8b). The influence of the meandering creek was evident. In particular, the creek was directly responsible for the small travel time distribution in its adjacent area.

[31] We also examined the particle travel time distribution in relation to the power law and exponential distributions with probability density functions defined as follows [*Clauset et al.*, 2009],

$$\text{power law: } p = (\alpha - 1)t_{\min}^{\alpha-1}t^{-\alpha}, \tag{2}$$

$$\text{exponential: } p = \lambda e^{\lambda t_{\min}}\mathrm{e}^{-\lambda t}, \tag{3}$$

where α and λ are the distribution parameters; $t_{\min}$ is the minimum travel time. Integrating the probability density functions gives the probability functions as follows:

$$\text{power law: } P_r(T \geq t) = t_{\min}^{\alpha-1}t^{1-\alpha}, \tag{4}$$

$$\text{exponential: } P_r(T \geq t) = e^{\lambda t_{\min}}\mathrm{e}^{-\lambda t}. \tag{5}$$

[32] Calculated travel times of all particles with and without flux weighting were ranked to give estimates of the probability $P_r(T \geq t)$. The results showed that neither equation (4) nor (5) fitted the estimated probability values (Figure 9). $t_{\min}$ was set to be the calculated minimum travel time in the fitting. Even with $t_{\min}$ as a free parameter, both equations still failed to fit the estimated probability values (results not shown).

[33] The power law distribution has been observed in studies of land-sourced chemicals in river systems [*Kirchner et al.*, 2000; *Wörman et al.*, 2007; *Cardenas*, 2008a], whereas the exponential distribution has been widely used

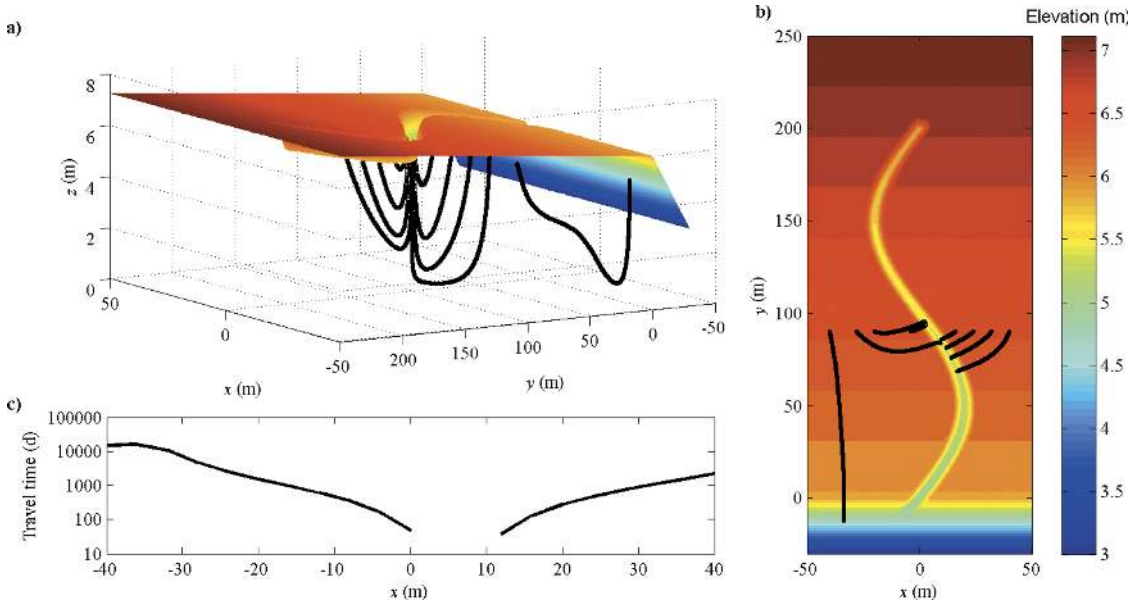

Figure 7. Particle tracking in the marsh soil: (a) 3-D particle trace and (b) plan view. The colored contour map represents the marsh topography (sediment surface elevation). The particles were released at $y = 90$ m (0.5 m soil depth). (c) The associated particle travel times. The x axis shows where the particle was released initially.

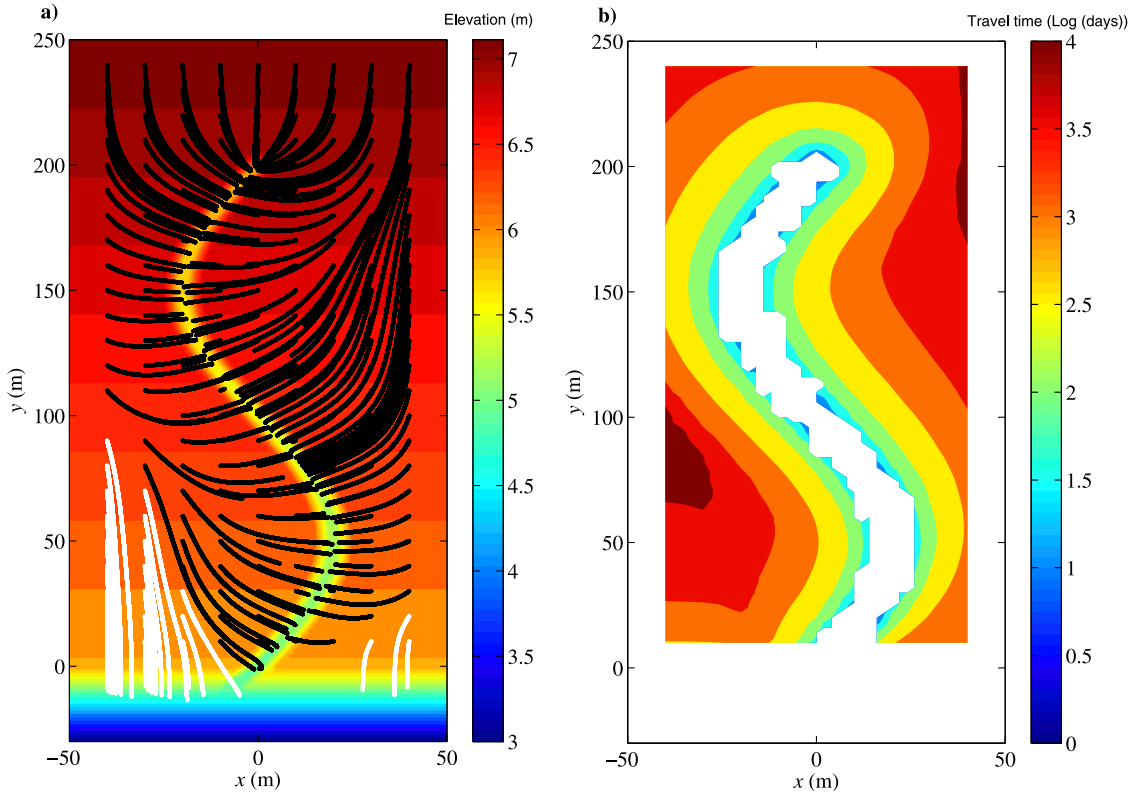

Figure 8. (a) Traces of particles initially released uniformly on the sediment surface and (b) associated particle travel times. The color bar in Figure 8a shows the sediment surface elevation, and that in Figure 8b shows the travel time in Log (days).

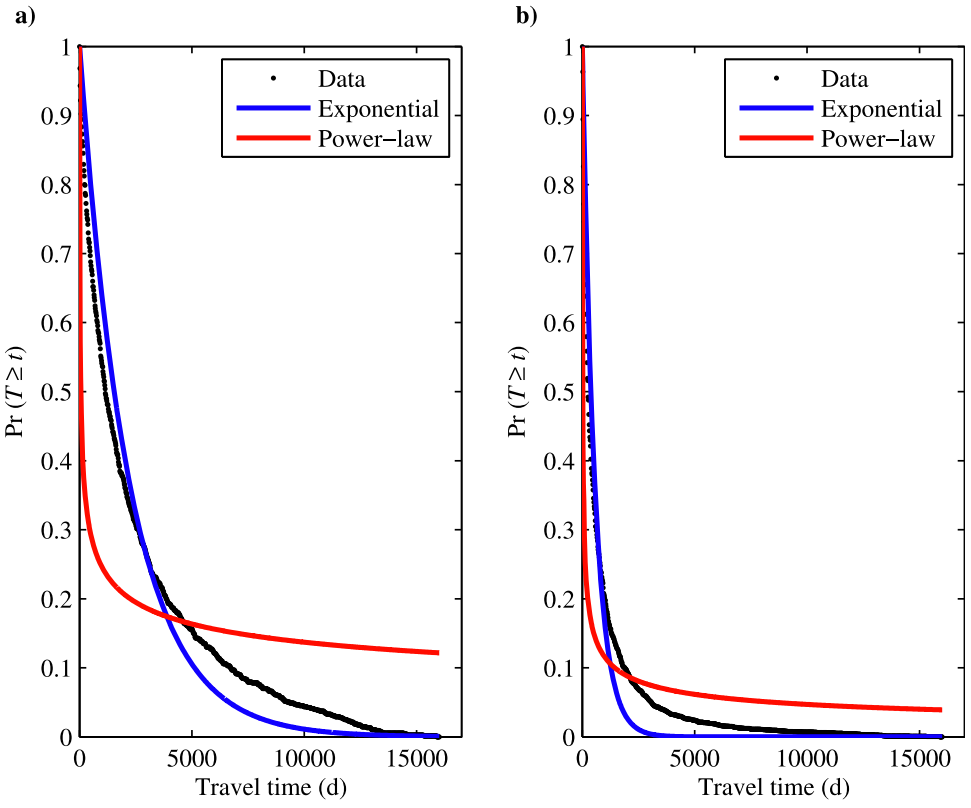

Figure 9. Probability of travel time greater than t ($T \geq t$): (a) for uniform particle numbers and (b) for particle numbers weighted by flux.

for describing travel time in aquifers [*McGuire and McDonnell*, 2006], and has been found to represent well the travel time behavior in a homogeneous unconfined aquifer [*Maloszewski and Zuber*, 1982]. However, the modeled creek-marsh system in this study did not exhibit characteristics of either a power law or an exponential travel time distribution.

3.3. Surface Water and Groundwater Interactions

[34] The results presented above have demonstrated the spatial and temporal characteristics of the pore water flow in the modeled creek-marsh system. In this section, fluxes across the interface between the surface water and groundwater bodies are quantified and analyzed based on the simulated flow.

[35] Total influx and efflux across the interface over the whole marsh area were calculated at different times over the tidal period (Figure 10). The total surface water flux across the creek-marsh edge (boundary BE in Figure 1), representing the surface water exchange between the creek-marsh system and main channel, was examined also. Affected by the sinusoidal (symmetric) tide, the temporal variation of this flux was largely symmetric (Figure 10b). Main channel water entered the creek-marsh system during the rising tide (6 to 12 h). Over the falling tide period, the marsh surface water discharged to the main channel. In contrast, the temporal variation of the flux across the marsh surface was highly asymmetric (Figure 10c). The results show that drainage of the whole subsurface system (with zero infiltration rate) started as the tidal level dropped below the marsh surface elevation at the top end of the creek. The total exfiltration increased gradually and stabilized after the surface water level fell below the marsh surface elevation at the border with the main channel (BE in Figure 1). As the tide rose, the exfiltration weakened and infiltration started. As the rising tidal water overtopped the sediment surface at marsh edge, a relatively large amount of surface water infiltrated the marsh soil where significant drainage to the steep channel bank had occurred prior to the rising tide, resulting in a total infiltration peak (around 8.4 h in Figure 10c). The infiltration dropped after the tidal water level passed this well drained area near the channel bank. As the tidal water continued to move landward into high elevation areas that had been drained to the creek, the infiltration increased again and to a high level just before the sea level reached the marsh surface at the top end of the creek. Subsequently, a relatively rapid decrease of the infiltration took place; as the whole marsh surface became submerged, both infiltration and exfiltration ceased. Overall, the exfiltration persisted over a large part of the tidal period except the period of total marsh submergence. In contrast, the infiltration occurred for a relatively short period but at a higher rate. While the infiltration largely took place through the unsaturated soil near the wetting front during the rising tide, the exfiltration occurred at the creek and on the exposed sediment surface during both rising and falling tide. The influx and efflux were integrated over the tidal period to give the total amount of water that moved into and out of the marsh soil. As the system was in a quasi-steady state, the two integrated fluxes over the tidal period were found to cancel out each other (both equal to 37.1 m^3, Table 2).

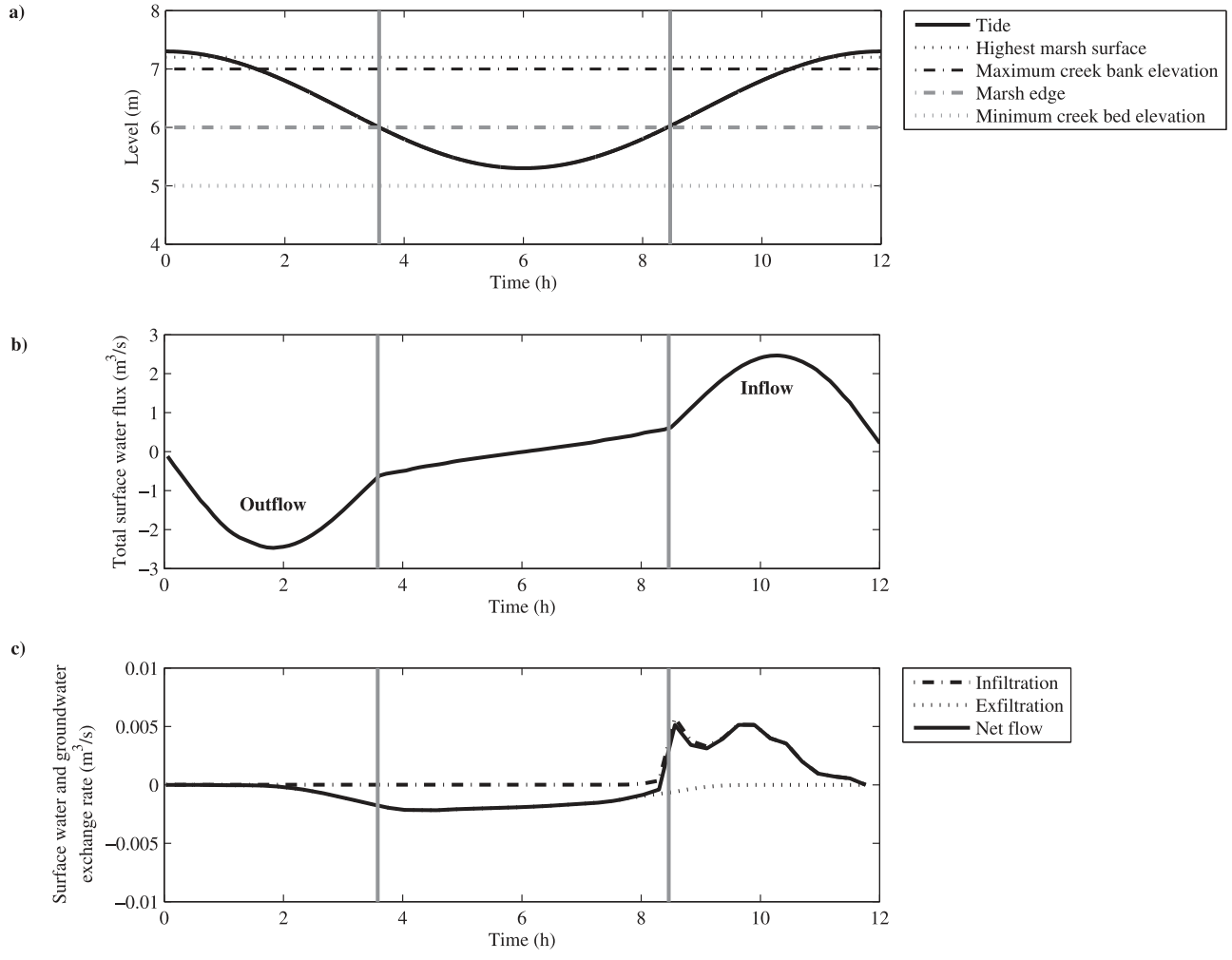

Figure 10. (a) Temporal changes of the tidal water level relative to local marsh surface elevations at various locations. (b) Temporal variations of the total surface water flux and (c) surface water and groundwater exchange rate. For Figures 10b and 10c, negative values are for outflow and positive values are for inflow. The period between the two vertical lines is during the exposure.

Table 2. Summary of Simulation Cases and Net Flux Results[a]

	Creek Topographic Parameters					Main Channel Topographic Parameters					
	L (m)	D (km km^{-2})	S	κ_{max}(m^{-1})	A_c(m^2)	L (m)	S	Q_{cr} (m^3)	Q_{mc} (m^3)	Q_T (m^3)	Q_{out} (m^3)
Case 1 (base case)	218	8.7	0.2	$\frac{\pi^2}{500}$	7	100	0.1	27.7	3.3	31.0	37.1
Case 2	205 (0.94[b])	16.4	0.4	$\frac{\pi^2}{1000}$	3.5	50	0.1	26.4 (0.95[c])	1.5 (0.45[d])	27.9	35.5
Case 3	132 (0.61[b])	10.6	0.2	$\frac{\pi^2}{250}$	7	100	0.2	16.8 (0.61[c])	4.4 (1.33[d])	21.2[e]	26.9

[a]L, length; D, creek density; S, bank slope; κ_{max}, maximum creek channel curvature; A_c, cross-sectional area; Q_{cr}, net efflux to the creek over the tidal period; Q_{mc}, net efflux to the main channel over the tidal period; Q_T, total net efflux over the tidal period; and Q_{out}, total intratidal outflow over the tidal period.

[b]Ratio of the creek length in case 2 or 3 to that in the base case.

[c]Ratio of the net efflux to the creek in case 2 or 3 to that in the base case.

[d]Ratio of net efflux to the main channel in case 2 or 3 to that in the base case.

[e]Negligible amount of water exited across the marsh surface.

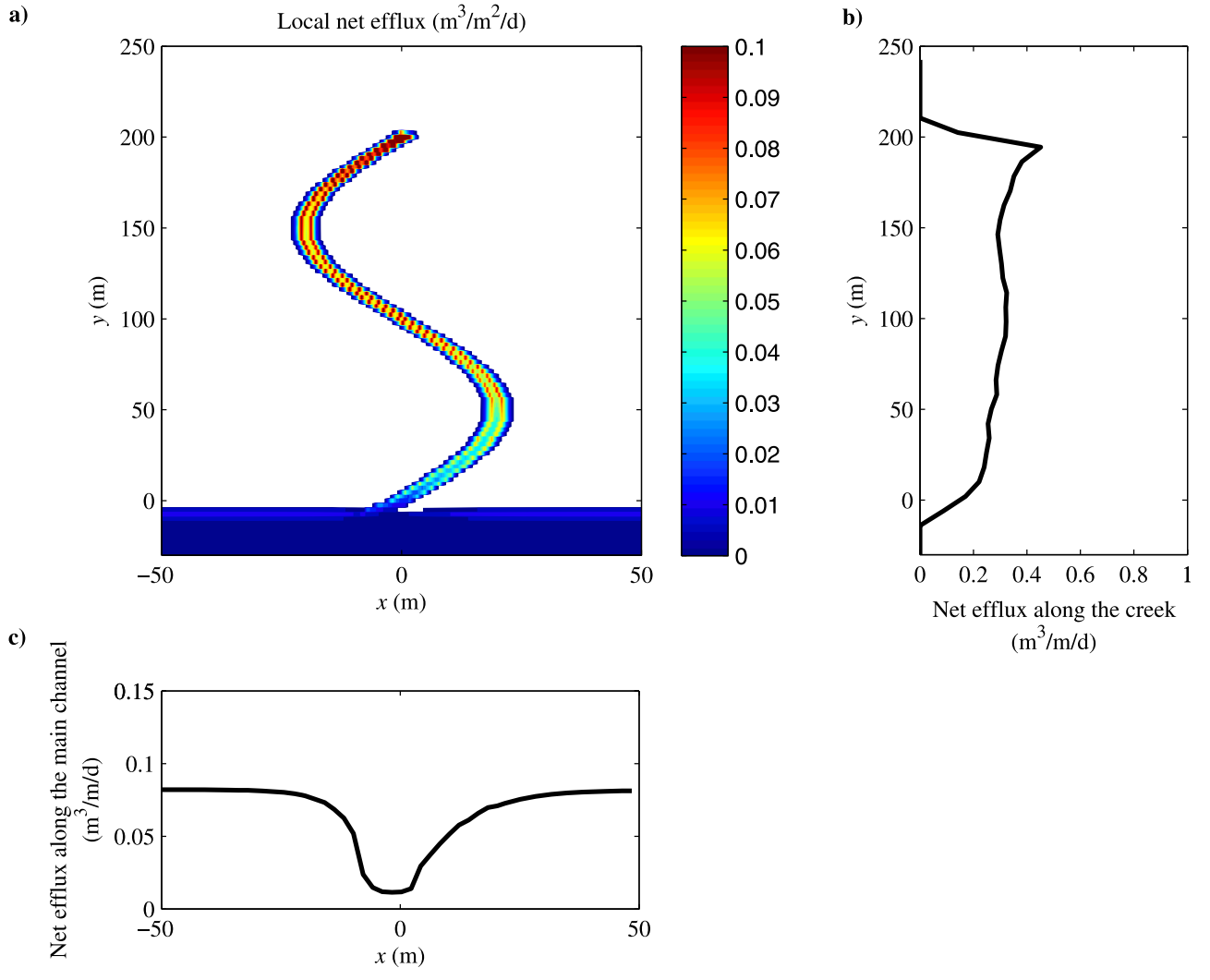

Figure 11. (a) Local net efflux (per unit area) across the interface of surface water and groundwater (in $m^3/m^2/d$). Variations of net efflux (b) along the creek and (c) along the main channel.

[36] Local net flux over the tidal period was also calculated (Figure 11). Drainage of pore water from the marsh soil occurred both along the creek and across the main channel bank. However, the main exit was the creek since 89% of the pore water in circulation drained to it (in agreement with flux-weighted particle tracking), compared with 11% across the main channel bank (Figure 11a). The local net flux in the creek area was integrated over the discharge zone width across the creek (in the x direction) to determine the variation of the efflux along the creek in the y direction (Figure 11b). The results showed that, except for the rapid change (to zero) near both the upper and lower end of the creek, the efflux variation was characterized by oscillations coupled with a slightly decreasing trend toward to the main channel. The oscillations, corresponding with the curvature of the creek channel, reflected the influence of the meander: a local efflux minimum occurred at the maximum creek channel curvature and vice versa (Figure 11b). The correspondence of the efflux rate with the creek channel curvature was linked to the effect of curvature on the drainage area of the local creek channel section, as indicated by particle traces (Figure 8a). Similarly, the local net flux in the main channel area was integrated across the channel to determine the efflux per unit channel length. Overall, the efflux rate along the main channel was significantly less than that along the creek. The results also showed competing influence of the creek and channel on the pore water drainage. Close to the creek, less water discharged through the main channel bank (Figure 11c).

[37] The efflux rates per unit length were integrated in the y and x direction to give the amount of net efflux over the tidal period to the creek and main channel, respectively. The net efflux to the creek was much larger than that to the main channel (Table 2). The net efflux included only the outflow of the tidally averaged circulation, excluding local recycling water (outflow of water that infiltrated the soil locally). Thus, the total net efflux (31.0 m^3) was less than the total amount of outflow based on the intratidal flow (37.1 m^3).

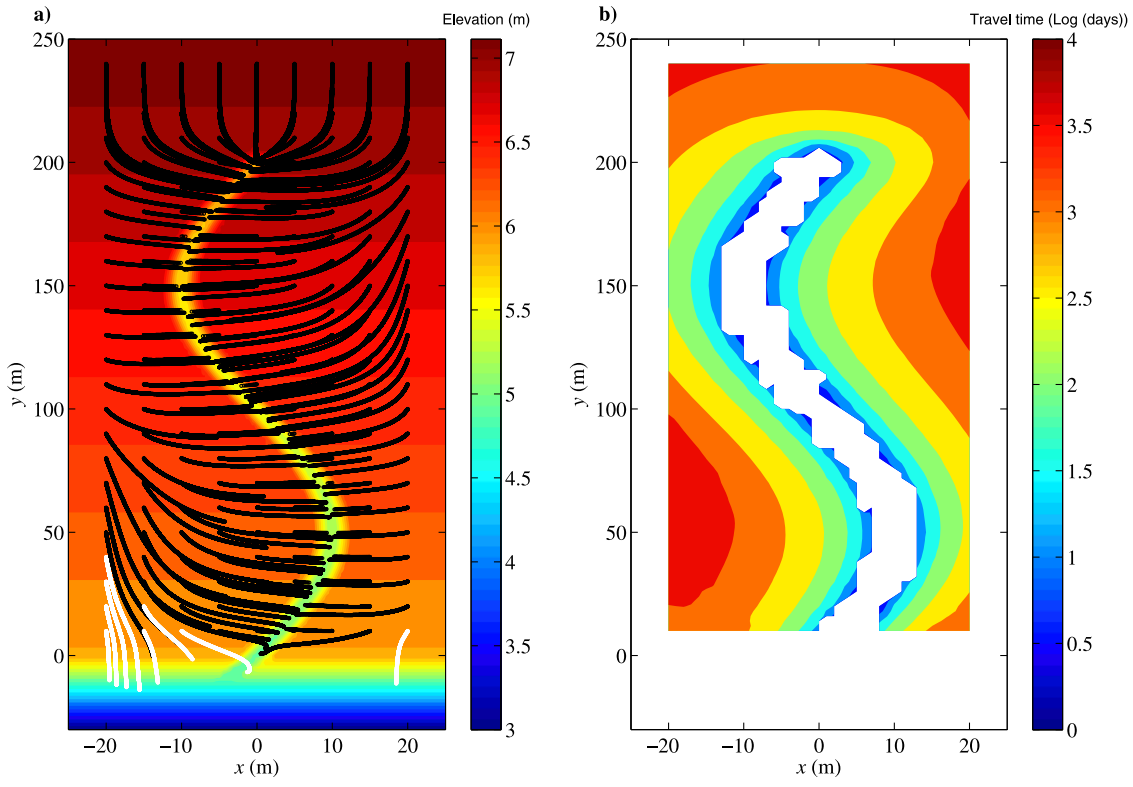

Figure 12. (a) Traces of particles initially released to the sediment surface uniformly, and (b) associated particle travel times. The legend in Figure 12a shows the sediment surface elevation, and the legend in Figure 12b shows the travel time in Log (days).

4. Sensitivity Analysis and Discussion

[38] The base simulation (case 1) showed that marsh topography influenced significantly the tide-induced pore water flow in the modeled creek-marsh system. To assess further topographic effects, two additional simulations were conducted with the model scale reduced by half in the along-channel (x; case 2) and cross-channel (y; case 3) directions, respectively. The resulting changes of the marsh topography are summarized in Table 2 together with key results. The scale reduction led to half marsh surface area and hence increased creek densities in both cases. While the slope of the creek bank increased by a factor of 2, the cross-sectional area and sinuosity (maximum curvature) of the creek in case 2 were reduced by half compared with the base case. The creek length was also reduced but only by a factor of 1.06. In contrast, case 3 simulated conditions of a relatively steep marsh surface and main channel bank with a shorter length and double sinuosity but the same cross-sectional area and bank slope of the creek (Table 2).

[39] The intratidal flow characteristics for both cases 2 and 3 were similar to those revealed by the base simulation. Consequently, the analysis focused on the particle tracking and net flux results. While the particle tracking in case 2 showed a similar circulation pattern to that in the base case, the effects of the creek on the pore water circulation/drainage became even more important (Figure 12). Over 96% (2308 out of 2397) of the particles released uniformly to the surface soil layer moved straight to the creek—an increase of 5% from the base case. The creek was also found to be the main exit (~95%) for the particles released in proportion to the local tidally averaged infiltration rate. Local net flux along the creek and main channel over the tidal period showed similar trends to those in the base case (Figure 13). However, no oscillation of the efflux was evident along the creek, suggesting that the creek meander, with reduced sinuosity, affected little the pore water drainage. The difference between the total efflux to the creek (26.4 m^3 over the tidal period) and main channel (1.5 m^3 over the tidal period) increased, ~95% of the total amount of circulating pore water drained to the creek compared with 89% in the base case, consistent with the particle tracking results.

[40] In contrast, case 3 witnessed a much more important role played by the main channel with an increased bank slope and shortened creek length. A relatively large number of particles (600 out of 2397; 25%) were discharged to the main channel (Figure 14). It is also interesting to note that, although particles (155 out of 2397; 6%) released in the upper inner marsh area (top right corner) moved out across the sediment surface, they traveled initially a long distance toward the main channel. This reflected the effect on the pore water flow given by the inclination of the marsh surface toward the main channel relative to the influence of the meander. Correspondingly, a considerable amount (4.4 m^3 out of 21.2 m^3 in total; 21%) of circulating pore water was drained to the main channel (Figure 15). The effect of the creek meander on the efflux variation along the creek was more profound than the base case. Convergence of circulating flow led to a discharge peak around $y = 50$ m, where the creek channel curvature was at the minimum (Figure 15). In contrast, local discharge minimums occurred around $y = 25$

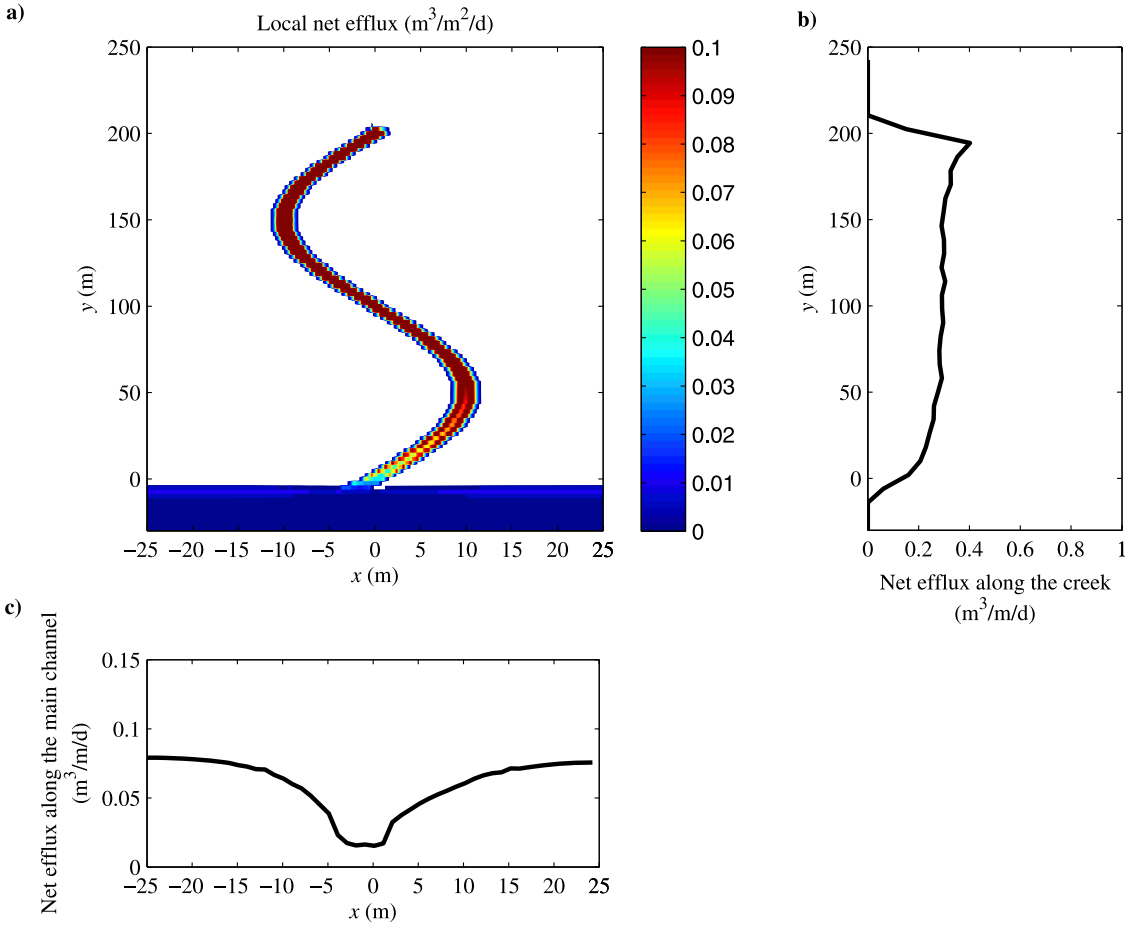

Figure 13. (a) Local net efflux (per unit area) across the interface of surface water and groundwater (in $m^3/m^2/d$). Variations of net efflux (b) along the creek and (c) along the main channel.

and 75 m where the creek channel curvature was at the maximum.

[41] The net effluxes to the creek and main channel in both cases 2 and 3 varied significantly from those in the base case (Table 2). Despite increased creek densities, the net effluxes to the creek decreased in both cases, exhibiting a strong correlation with the reduced creek lengths. The proportional reduction of the creek efflux in case 3 relative to the base case matched the proportional reduction of the creek length. The creek efflux in case 2, which was also influenced by an increased creek bank slope and decreased cross-sectional area, was not reduced to the same extent as that of the creek length reduction. In contrast, the efflux to the main channel behaved in a more complicated way. While the channel efflux was reduced due to the channel length reduction in case 2, it increased as a result of enhanced channel drainage capacity with a larger bank slope in case 3.

[42] These results suggest that the multiscale flow characteristics shown by the base simulation are fundamental of the modeled creek-marsh system. The dominance of the different pore water circulation and particle travel paths depends on the competing influences of the creek and main channel. Such influences are represented by topographic parameters including the creek and main channel bank slope, marsh surface slope, and the creek length, channel curvature, and cross-sectional area. These parameters also combine to influence the amount of water in exchange between the marsh soil and coastal water with drainage at both the creek and main channel.

5. Conclusions

[43] Numerous studies have been conducted to examine the behavior and functionalities of salt marshes and other intertidal wetlands, including recent modeling work on the tide-induced pore water flow in marsh soils based on 2-D vertical sections perpendicular to the creek. While the previous work sheds some light on pore water circulation near the creek, little is known about the overall flow characteristics, in particular, the role played by multiscale marsh topography in modulating the flow. This study represents a first attempt to model 3-D pore water flow in a creek-marsh system, taking into account surface water and groundwater interactions. Using a synthetic 3-D salt marsh model with an embedded meandering creek, we explored intratidal pore water flow dynamics, tidally averaged flow, and associated particle paths and fluxes across the marsh surface.

[44] The study demonstrated a dynamic, multiscale 3-D flow in the marsh soil, which corresponded with the tidal forcing and various topographic variations built in the model. The flow was characterized by pore water circulation

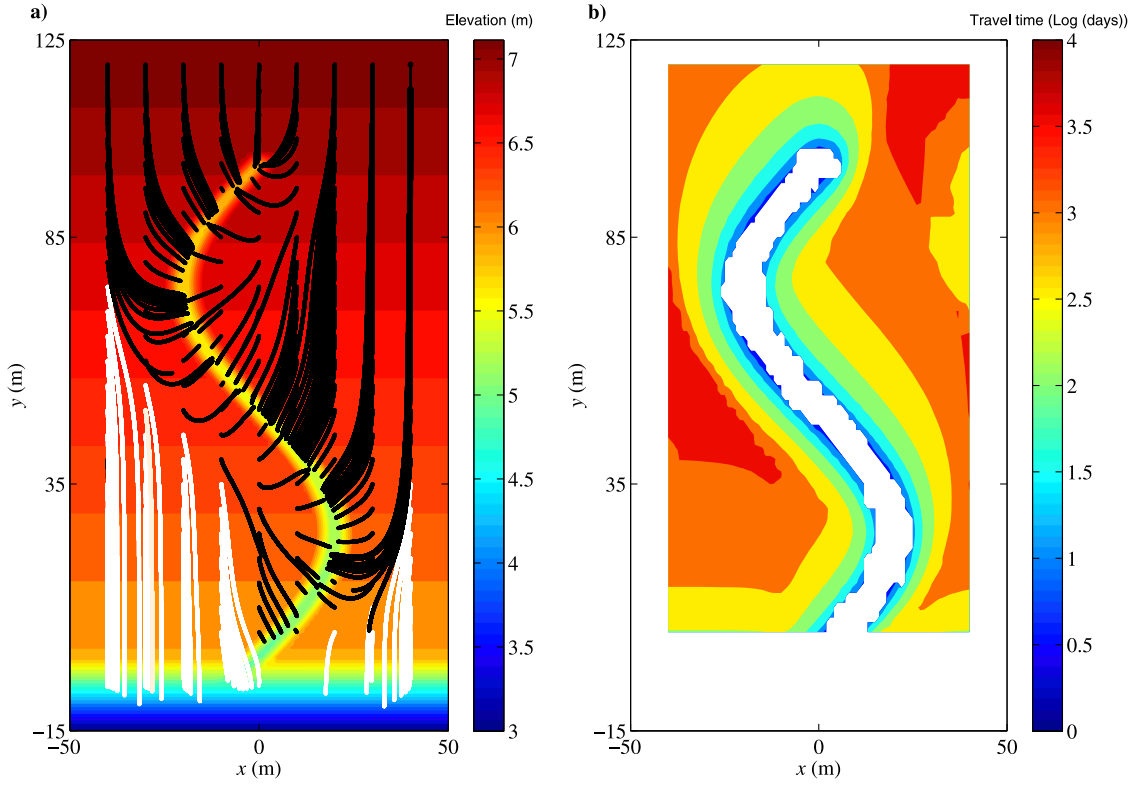

Figure 14. (a) Traces of particles initially released to the sediment surface uniformly and (b) associated particle travel times. The legend in Figure 14a shows the sediment surface elevation, and the legend in Figure 14b shows the travel time in Log (days).

that connected surface water infiltration through the marsh platform during submergence and drainage at both the creek and main channel as the tide receded. The circulating flow varied greatly in space and time. Particles traveling through the circulation paths re-emerged over time scales that differed over orders of magnitude, depending on the locations where particles were released. In many ways, the salt marsh behaved like a shallow groundwater system in a humid region with a "gaining" river/stream. The creek, like the "gaining" river, drained the marsh largely. A certain amount of pore water discharged to the main channel directly, similar to coastal groundwater discharge to the ocean [*Moore*, 1999; *Li et al.*, 1999; *Xin et al.*, 2010b].

[45] The pore water flow characteristics revealed in this study have the following key implications for future investigations of marsh ecohydrology:

[46] 1. Three dimensionality is a fundamental feature of the simulated pore water flow in the modeled creek-marsh system, largely due to the combined influences of the meandering creek and main channel. In real marshes with creek/channel networks embedded, the pore water drainage to creeks and channels is likely to behave in an even more complex way with profound 3-D patterns, which would require 3-D models for the purpose of simulation. Two-dimensional models may still be applied to examine the local tidally driven pore water circulation close to individual, "remote" creek/channel sections; however, these models would not be able to simulate the overall 3-D pore water flow and drainage in the marsh system, particularly in areas near the creek/channel junctions and large creek meanders.

[47] 2. Multiple scales are evident in the simulated pore water flow. Under the influence of the marsh topography, the pore water circulation occurs over a wide range of spatial and temporal scales. As the pore water in circulation largely originates from surface water, the multiscale circulation is likely to play an important role in the chemical exchange between the marsh soil and coastal surface water. While the small scale circulation produces the greater discharge, the large scale circulation facilitates longer interactions of circulating water with the soil, which may lead to significant modifications of chemical composition of the pore water and chemical fluxes at the circulation outlet.

[48] 3. The dominance of the creek over the main channel in draining the marsh soil is also a key feature of the modeled creek-marsh system. Although the discharges to the creek and main channel varied under the influences of a range of topographic parameters, the creek in the three considered cases provided the main drainage outlet for the recirculating water. The drainage to the creek is likely to produce significant fluxes of chemicals sourced from the marsh soil. Therefore, modeling of chemical transport in the creek water is important for determining ultimately the flux from the marsh to the coastal sea. Such modeling would need to resolve coupled 3-D surface water and pore water flow and solute transport processes in the marsh system.

[49] While the present study has generated insights into pore water flow in marsh soils, further investigations should be conducted to examine other factors that were not considered. These include evapotranspiration, precipitation, and regional flow (as shown in Figure 1), which all provide

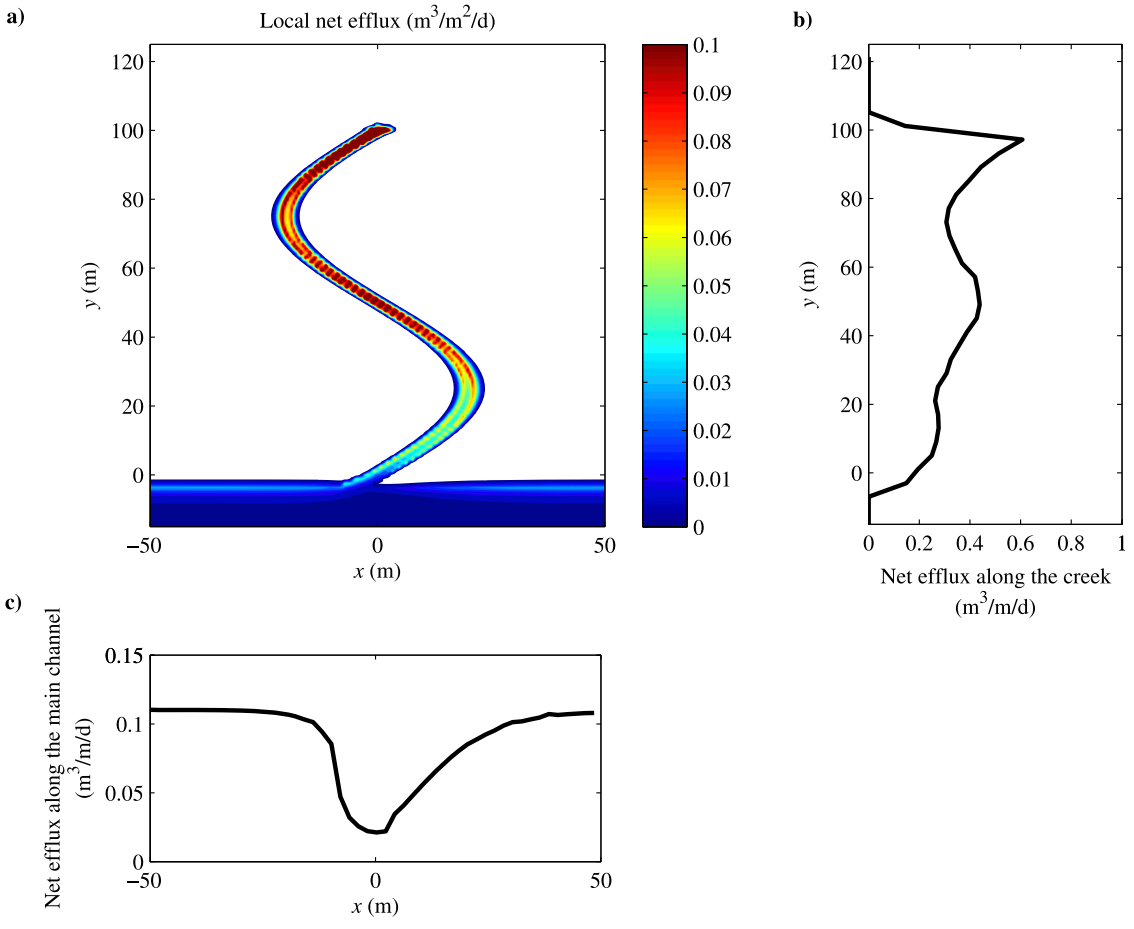

Figure 15. (a) Local net efflux (per unit area) across the interface of surface water and groundwater (in $m^3/m^2/d$). Variations of net efflux (b) along the creek and (c) along the main channel.

additional forcing on the flow and transport in the marsh system. The interplay of these factors with the tide is likely to lead to more complex flow behavior. The modeled marsh was composed of a homogeneous sandy loam. In reality, heterogeneous marsh soils are the norm. For example, a two-layer soil structure has been found in many marshes where a fine-grained mud layer overlies a sandy loam layer. Such a soil stratigraphy would affect significantly the pore water flow [*Gardner*, 2007; *Xin et al.*, 2009]. In addition, the model considered only a single creek without a network included. Although the simulated creek density was similar to observations, the absence of the creek network is likely to have resulted in simplifications in not only the pore water flow patterns but also in the surface water hydrodynamics. Furthermore, we considered a smooth marsh surface. Local topographic variations, at smaller scales, may induce "skin circulation" near the sediment surface. Compared with the "body circulation" examined here, the skin circulation is characterized by shorter flow paths and travel times [*Billerbeck et al.*, 2006]. Tidal oscillations with multiple constituents such as spring and neap tides (involving semidiurnal solar and lunar tides) would complicate further the flow in the marsh, possibly with upper areas inundated only during the spring tides, much less frequently than the simulated condition. These gaps provide directions for future studies to advance our understanding of salt marshes. The key to unraveling this complex hydrological system is proper consideration of surface water and groundwater interactions that underpin the marsh's behavior and functionalities.

[50] **Acknowledgments.** This research was supported by the Australian Research Council (DP0988718) and the National Natural Science Foundation of China (51009059). P.X. acknowledges an Early Career Researcher grant provided by The University of Queensland (603275). The authors acknowledge valuable comments from three anonymous reviewers and the managing associate editor, which led to significant improvement of the paper.

References

Allen, J. R. L. (2000), Morphodynamics of Holocene salt marshes: A review sketch from the Atlantic and Southern North Sea coasts of Europe, *Quat. Sci. Rev.*, *19*(12), 1155–1231.

Alley, W. M., R. W. Healy, J. W. LaBaugh, and T. E. Reilly (2002), Flow and storage in groundwater systems, *Science*, *296*, 1985–1990.

Billerbeck, M., U. Werner, L. Polerecky, E. Walpersdorf, D. deBeer, and M. Huettel (2006), Surficial and deep pore water circulation governs spatial and temporal scales of nutrient recycling in intertidal sand flat sediment, *Marine Ecol. Prog. Ser.*, *326*, 61–76.

Cardenas, M. B. (2008a), Surface water-groundwater interface geomorphology leads to scaling of residence times, *Geophys. Res. Lett.*, *35*(8), L08402, doi:10.1029/2008GL033753.

Cardenas, M. B. (2008b), The effect of river bend morphology on flow and timescales of surface water-groundwater exchange across pointbars, *J. Hydrol.*, *362*(1–2), 134–141.

Cardenas, M. B. (2009), Stream-aquifer interactions and hyporheic exchange in gaining and losing sinuous streams, *Water Resour. Res.*, *45*, W06429, doi:10.1029/2008WR007651.

Carsel, R. F., and R. S. Parrish (1988), Developing joint probability distributions of soil water retention characteristics, *Water Resour. Res.*, *24*(5), 755–769, doi:10.1029/WR024i005p00755.

Chapman, V. J. (1960), *Salt Marshes and Salt Deserts of the World*, Leonard Hill, London.

Chmura, G. L., S. C. Anisfeld, D. R. Cahoon, and J. C. Lynch (2003), Global carbon sequestration in tidal, saline wetland soils, *Global Biogeochem. Cycles*, *17*(4), 1111, doi:10.1029/2002GB001917.

Clauset, A., C. R. Shalizi, and M. E. J. Newman (2009), Power-law distributions in empirical data, *SIAM Rev.*, *51*(4), 661–703.

Colmer, T. D., and T. J. Flowers (2008), Flooding tolerance in halophytes, *New Phytologist*, *179*(4), 964–974.

D'Alpaos, A., S. Lanzoni, M. Marani, and A. Rinaldo (2007), Landscape evolution in tidal embayments: Modeling the interplay of erosion, sedimentation, and vegetation dynamics, *J. Geophys. Res.*, *112*(F1), F01008, doi:10.1029/2006JF000537.

Francis, B. A., L. K. Francis, and M. B. Cardenas (2010), Water table dynamics and groundwater-surface water interaction during filling and draining of a large fluvial island due to dam-induced river stage fluctuations, *Water Resour. Res.*, *46*, W07513, doi:10.1029/2009WR008694.

Gardner, L. R. (2005), Role of geomorphic and hydraulic parameters in governing pore water seepage from salt marsh sediments, *Water Resour. Res.*, *41*(7), W07010, doi:10.1029/2004WR003671.

Gardner, L. R. (2007), Role of stratigraphy in governing pore water seepage from salt marsh sediments, *Water Resour. Res.*, *43*(7), W07502, doi:10.1029/2006WR005338.

Harvey, J. W., and W. E. Odum (1990), The influence of tidal marshes on upland groundwater discharge to estuaries, *Biogeochemistry*, *10*(3), 217–236.

Howes, B. L., and D. D. Goehringer (1994), Porewater drainage and dissolved organic carbon and nutrient losses through the intertidal creekbanks of a New England salt marsh, *Marine Ecol. Prog. Ser.*, *114*(3), 289–301.

Howes, B. L., R. W. Howarth, J. M. Teal, and I. Valiela (1981), Oxidation-reduction potentials in a salt marsh: Spatial patterns and interactions with primary production, *Limnol. Oceanogr.*, *26*(2), 350–360.

Jordan, T. E., and D. L. Correll (1985), Nutrient chemistry and hydrology of interstitial water in brackish tidal marshes of Chesapeake Bay, *Estuarine, Coastal Shelf Sci.*, *21*(1), 45–55.

Kirchner, J. W., X. Feng, and C. Neal (2000), Fractal stream chemistry and its implications for contaminant transport in catchments, *Nature*, *403*(6769), 524–527.

Li, H. L., L. Li, and D. Lockington (2005), Aeration for plant root respiration in a tidal marsh, *Water Resour. Res.*, *41*(6), W06023, doi:10.1029/2004WR003759.

Li, L., D. A. Barry, F. Stagnitti, and J. Y. Parlange (1999), Submarine groundwater discharge and associated chemical input to a coastal sea, *Water Resour. Res.*, *35*(11), 3253–3259, doi:10.1029/1999WR900189.

Maloszewski, P., and A. Zuber (1982), Determining the turnover time of groundwater systems with the aid of environmental tracers: 1. Models and their applicability. *J. Hydrol.*, *57*(3–4), 207–231.

Mao, X., P. Enot, D. A. Barry, L. Li, A. Binley, and D. S. Jeng (2006), Tidal influence on behaviour of a coastal aquifer adjacent to a low-relief estuary, *J. Hydrol.*, *327*(1–2), 110–127.

Marani, M., S. Silvestri, E. Belluco, N. Ursino, A. Comerlati, O. Tosatto, and M. Putti (2006), Spatial organization and ecohydrological interactions in oxygen-limited vegetation ecosystems, *Water Resour. Res.*, *42*(6), W06D06, doi:10.1029/2005WR004582.

McGuire, K. J., and J. J. McDonnell (2006), A review and evaluation of catchment transit time modeling, *J. Hydrol.*, *330*(3–4), 543–563.

Mendelssohn, I. A., K. L. McKee, and W. H. Patrick (1981), Oxygen deficiency in Spartina alterniflora roots: Metabolic adaptation to anoxia, *Science*, *214*(4519), 439–441.

Moore, W. S. (1999), The subterranean estuary: A reaction zone of ground water and sea water, *Marine Chem.*, *65*(1–2), 111–125.

Novakowski, K. I., R. Torres, L. R. Gardner, and G. Voulgaris (2004), Geomorphic analysis of tidal creek networks, *Water Resour. Res.*, *40*(5), W05401, doi:10.1029/2003WR002722.

Reeves, H. W., P. M. Thibodeau, R. G. Underwood, and L. R. Gardner (2000), Incorporation of total stress changes into the groundwater model SUTRA, *Ground Water*, *38*(1), 89–98.

Rinaldo, A., E. Belluco, A. D'Alpaos, A. Feola, S. Lanzoni, and M. Marani (2004), Tidal networks: form and function, Ecogeomorphology of tidal marshes, in *Coastal and Estuarine Monograph*, edited by S. Fagherazzi, M. Marani and L. K. Blum, pp. 75–92, American Geophysical Union, Washington, D. C.

Robinson, C., L. Li, and D. A. Barry (2007), Effect of tidal forcing on a subterranean estuary, *Adv. Water Resour.*, *30*(4), 851–865.

Robinson, C., A. Brovelli, D. A. Barry, and L. Li (2009), Tidal influence on BTEX biodegradation in sandy coastal aquifers, *Adv. Water Resour.*, *32*(1), 16–28.

Simonini, P., and S. Cola (2002), Some pore pressure measurements at the marsh of S. Felice in the Venice lagoon, in *Scientific Research and Safeguarding of Venice, CORILA Research Program 2001 Results*, Ist. Veneto di Sci. Lett. ed Arti, Venice, Italy.

Smith, A. J., and J. V. Turner (2001), Density-dependent surface water–groundwater interaction and nutrient discharge in the Swan-Canning Estuary, *Hydrol. Process.*, *15*(13), 2595–2616.

Teal, J. M. (1962), Energy flow in the salt marsh ecosystem of Georgia, *Ecology*, *43*(4), 614–624.

Tobias, C. R., S. A. Macko, I. C. Anderson, E. A. Canuel, and J. W. Harvey (2001), Tracking the fate of high concentration groundwater nitrite plume through a fringing marsh: A combined groundwater tracer and in situ isotope enrichment study, *Limnol. Oceanogr.*, *46*(8), 1977–1989.

Torres, R., and R. Styles (2007), Effects of topographic structure on salt marsh currents, *J. Geophys. Res.*, *112*(F2), F02023, doi:10.1029/2006JF000508.

Ursino, N., S. Silvestri, and M. Marani (2004), Subsurface flow and vegetation patterns in tidal environments, *Water Resour. Res.*, *40*(5), W05115, doi:10.1029/2003WR002702.

Valiela, I., and J. M. Teal (1979), The nitrogen budget of a salt marsh ecosystem, *Nature*, *280*(5724), 652–656.

Valiela, I., J. M. Teal, S. B. Volkmann, C. M. Cogswell, and R. A. Harrington (1980), On the measurement of tidal exchanges and groundwater flow in salt marshes, *Limnol. Oceanogr.*, *25*(1), 187–192.

van Genuchten, M. Th. (1980), A closed form equation for predicting the hydraulic conductivity of unsaturated soils, *Soil Sci. Soc. Am. J.*, *44*(5), 892–898.

Vernberg, F. J. (1993), Salt-marsh processes: A review, *Environ. Toxicol. Chem.*, *12*(12), 2167–2195.

Voss, C. I., and A. M. Provost (2008), A model for saturated-unsaturated, variable-density ground-water flow with solute or energy transport, U.S. Geological Survey, Water-Resources Investigations Report 02-4231.

Wang, Z., J. Feyen, D. R. Nielsen, and M. Th. van Genuchten (1997), Two phase flow infiltration equations accounting for air entrapment effects, *Water Resour. Res.*, *33*(12), 2759–2767, doi:10.1029/97WR01708.

Wilson, A. M., and L. R. Gardner (2006), Tidally driven groundwater flow and solute exchange in a marsh: Numerical simulations, *Water Resour. Res.*, *42*(1), W01405. doi:10.1029/2005WR004302.

Wörman, A., A. I. Packman, L. Marklund, J. W. Harvey, and S. H. Stone (2007), Fractal topography and subsurface water flows from fluvial bedforms to the continental shield, *Geophys. Res. Lett.*, *34*(7), L07402, doi:10.1029/2007GL029426.

Xin, P., G. Jin, L. Li, and D. A. Barry (2009), Effects of crab burrows on pore water flows in salt marshes, *Adv. Water Resour.*, *32*(3), 439–449.

Xin, P., B. Gibbes, L. Li, Z. Song, and D. Lockington (2010a), Soil saturation index of salt marshes subjected to spring-neap tides: A new variable for describing marsh soil aeration condition, *Hydrol. Process.*, *24*(18), 2564–2577.

Xin, P., C. Robinson, L. Li, D. A. Barry, and R. Bakhtyar (2010b), Effects of wave forcing on a subterranean estuary, *Water Resour. Res.*, *46*, W12505, doi:10.1029/2010WR009632.

Yuan, L., P. Xin, J. Kong, L. Li, and D. Lockington (2011), A coupled model for simulating surface water and groundwater interactions in coastal wetlands, *Hydrol. Process.*, doi:10.1002/hyp.8079.

Zhang, Y. L., A. M. Baptista, and E. P. Myers (2004), A cross-scale model for 3D baroclinic circulation in estuary-plume-shelf systems: I. Formulation and skill assessment, *Continental Shelf Res.*, *24*(18), 2187–2214.

D. A. Barry, Laboratoire de technologie écologique, Institut d'ingénierie de l'environnement, Faculté de l'environnement naturel, architectural et construit, Ecole Polytechnique Fédérale de Lausanne, Station 2, CH-1015, Lausanne, Switzerland. (andrew.barry@epfl.ch)

L. Li and P. Xin, National Centre for Groundwater Research and Training, School of Civil Engineering, University of Queensland, Qld, Australia. (p.xin@uq.edu.au; l.li@uq.edu.au)

L.-R. Yuan, School of Engineering, University of Sun Yat-Sen, GuangZhou, China. (yuanlr@mail.sysu.edu.cn)